Abdominal Applications of Quantitative 4D Flow MRI

Thekla H. Oechtering[a,b], **Grant S. Roberts**[c], **Nikolaos Panagiotopoulos**[a,b], **Oliver Wieben**[a,c], **Alejandro Roldán-Alzate**[a,d,e], **Scott B. Reeder**[a,c,d,e,f]

[a]University of Wisconsin, Department of Radiology, Madison, WI, United States

[b]Universität zu Lübeck, Department of Radiology, Luebeck, Germany

[c]University of Wisconsin, Department of Medical Physics, Madison, WI, United States

[d]University of Wisconsin, Department of Mechanical Engineering, Madison, WI, United States

[e]University of Wisconsin, Department of Biomedical Engineering, Madison, WI, United States

[f]University of Wisconsin, Department of Emergency Medicine, Madison, WI, United States

Abstract

4D flow MRI is a quantitative MRI technique that allows the comprehensive assessment of time-resolved hemodynamics and vascular anatomy over a 3-dimensional imaging volume. It effectively combines several advantages of invasive and non-invasive imaging modalities like ultrasound, angiography, and computed tomography in a single MRI acquisition and provides an unprecedented characterization of velocity fields acquired non-invasively in vivo.

Functional and morphological imaging of the abdominal vasculature is especially challenging due to its complex and variable anatomy with a wide range of vessel calibers and flow velocities and the need for large volumetric coverage. Despite these challenges, 4D flow MRI is a promising diagnostic and prognostic tool as many pathologies in the abdomen are associated with changes of either hemodynamics or morphology of arteries, veins, or the portal venous system.

In this review article, we will discuss technical aspects of the implementation of abdominal 4D flow MRI ranging from patient preparation and acquisition protocol over post-processing and quality control to final data analysis. In recent years, the range of applications for 4D flow in the abdomen has increased profoundly. Therefore, we will review potential clinical applications and address their clinical importance, relevant quantitative and qualitative parameters, and unmet challenges.

Keywords

magnetic resonance imaging; abdomen; hemodynamics; portal venous system; aorta; phase contrast MRI

Introduction to 4D flow MRI

4D flow MRI is a unique phase contrast MRI technique that measures velocities in a three-dimensional volume in three directions, resolved in time, hence "4D" [1, 2]. There is a broad range of possible indications for quantitative 4D flow MRI in the abdomen that span from pathologies of the aorta and its branch vessels to portal venous pathologies and even to uteroplacental vascular disease [3, 4]. In clinical routine, ultrasound and 2D flow MRI methods are used for hemodynamic analysis in abdominal pathologies whereas cross-sectional imaging, i.e., CT, MRI, and ultrasound, is often the preferred choice for anatomic evaluation of abdominal vessels. Compared to CT and conventional MRI methods, 4D flow MRI can gather both hemodynamic and anatomical information within a single acquisition. Unlike ultrasound, 4D flow MRI has minimal to no operator dependence, with easy prescription of a 3D volume of interest, and characterization of the velocity vector in all three spatial directions. Unlike 2D flow MRI, it offers the ability to interrogate vessels retrospectively, even with complex anatomy such as varices. This "image once, post-process many" paradigm is a major advantage of 4D flow MRI strategies (Table 1).

4D flow MRI-derived flow measurements in the abdomen are well-validated against ultrasound flow measurements [5–7] and 2D flow MRI [8–10]. Abdominal 4D flow MRI has demonstrated good interobserver variability and scan-rescan reproducibility after several months [11] as well as internal consistency using conservation of mass principles [12–15]. In addition to providing phase contrast images that capture the velocity of flowing blood, magnitude images and phase-contrast complex difference angiograms with high resolution encompass anatomical information. For example, non-contrast 4D flow based renal artery angiography in the clinical setting of suspected renal artery stenosis, compared favorably with contrast-enhanced MR angiography (MRA) [16].

Historically, the application of 4D flow MRI in the abdomen was and is still underutilized compared to the aorta, heart, head, and neck. The reasons for a relative lack of adoption in the abdomen are not entirely clear, but most likely related to technical difficulties, rather than clinical relevance, which is considerable. 4D flow MRI in the abdomen is more demanding and combines major challenges of other regions. These include the need for both cardiac gating and respiratory gating or compensation, large and variable volumetric coverage, and variable anatomy with small caliber vessels (e.g., hepatic artery branches). Moreover, abdominal vascular anatomy is complex with common anatomical variants and combines arterial, portal-venous, and venous flow velocities that would ideally be captured simultaneously. New acquisition and post-processing techniques increasingly address these challenges. In this article, we will give an overview over technical aspects of abdominal 4D flow MRI and discuss potential clinical applications.

Technical aspects

Patient preparation

Many studies have shown dramatic changes in abdominal flow velocities and volumes before and after a meal not only in the portal venous system but also in the arterial system [13, 14]. The literature typically reports fasting periods between 3 and 12 hours [12, 13, 17–19] prior to abdominal flow studies. A consistent fasting period will allow the standardization of normal reference ranges and comparison to follow-up studies. Therefore, we recommend standardizing patient preparation for abdominal 4D flow MRI and recommend a fasting period of at least 5 hours prior to the exam. Adequate fasting is particularly important if the patient is to undergo a meal challenge to examine differences in pre- and postprandial states.

To analyze the hemodynamic response to a meal challenge, it is reasonable to compare pre- and postprandial hemodynamics before and after standardized food intake. Frequently, nutrition shakes containing concentrated calories and protein are used to induce a consistent meal stimulus [13, 14]. The maximum response to a meal challenge in the superior mesenteric artery can be measured between 15 and 60 minutes after the meal depending on composition and energy content of the meal. Notably, blood flow in the superior mesenteric artery is reported to increase by 60% to 250% in healthy subjects. Increase in blood flow and velocity is more pronounced after fat-rich meals compared to carbohydrate meals [20, 21]. Fat-rich meals also induce a more prolonged hyperemia in the mesenteric vessels remaining at 79% above baseline 180 minutes after the meal [21]. We recommend ingestion of a standardized meal, such as a high-calorie nutrition shake, followed by 4D flow imaging after 20 minutes while other groups prefer delays of up to 60 minutes [22].

It must be noted that 4D flow MRI may not be well suited for acute situations such as detection of active bleeding, as acquisition, image reconstruction, and post-processing can require considerable time, for example compared to CT. Moreover, due to cardiac triggering, 4D flow MRI only gathers repetitive flow patterns that occur unchanged in every cardiac cycle. This is typically not the case in active bleeding that may vary independently from the cardiac cycle.

Acquisition protocol

4D flow MRI uses a cardiac gated, 3D phase contrast gradient-echo sequence to simultaneously acquire flow velocities in three spatial directions and anatomic information. A minimum of four acquisitions with varying bipolar gradient pairs for motion encoding is required to properly estimate velocities in three spatial directions [23]. The data are typically reconstructed into three phase contrast datasets with orthogonal velocity encodings in superior-inferior, right-left, and anterior-posterior direction as well as a magnitude dataset (Fig. 1). Often, a complex difference dataset is also reconstructed as a PC angiogram that combines information of the absolute velocity without information of direction, i.e.: speed and magnitude [16]. This can be easily reconstructed using complex difference angiography, which provides a useful means of non-contrast anatomical angiography. Most major MRI vendors offer 4D flow MRI as a product or research sequence which can be acquired on both

1.5T and 3T systems. Acquisition parameters and properties can differ significantly between different sequences.

Several spatial encoding techniques have been exploited and validated for abdominal 4D flow MRI, namely Cartesian and non-Cartesian techniques that fill the k-space either line per line (Cartesian) [6, 7, 9, 10], radially [5, 12], or spirally [24, 25]. Typically, vendor provided sequences use Cartesian sampling with different acceleration methods such as parallel imaging [6, 26], kt-acceleration [27, 28], or compressed sensing [29, 30]. In comparison to traditional Cartesian k-space sampling, the advantage of radial or spiral undersampling techniques are decreased motion sensitivity [31, 32], shorter echo times, and favorable properties for acceleration of data acquisition allowing for a decreased scan time or a larger imaging volume and/or improved spatial and/or temporal resolution. The main disadvantage of non-Cartesian methods is the need for more complex and computationally demanding image reconstruction. Typical acquisition times for respiratory gated abdominal flow imaging range between 7 and 23 minutes [6, 7, 9, 15, 33] for Cartesian, and 10 to 12 minutes for radial sampling [12–14, 17, 34, 35].

Ideally, the whole abdomen would be covered with an isotropic spatial resolution of 5–6 voxels per diameter of the vessels of interest [2]. Due to acquisition time constraints, this is not yet possible for small branches of important vessels like small renal arteries or branches of the hepatic arteries. Typical voxel sizes reported in the literature are about 1.5–3mm in-plane and 2–4mm through plane for Cartesian sequences and approximately 5–10 times smaller voxels with radial sequences that can achieve 1.25 mm isotropic spatial resolution. In addition, the imaging volume is larger and acquisition times tend to be shorter in radial acquisitions compared to Cartesian acquisitions. Typical acquisition parameters reported in the literature for different vessels of interest are compiled in Table 2.

To capture flow velocities throughout the cardiac cycle, cardiac synchronization, typically performed using ECG gating is required. Ideally, retrospective ECG triggering should be used to facilitate coverage of the entire cardiac cycle. If not available, prospective cardiac gating is a good alternative, although this approach typically misses the last part of diastole. However, in this case it is recommended to adjust quantitative measurements that are based on the whole cardiac cycle (e.g., flow volumes) based on the percentage of the cardiac cycle that was acquired and the heart rate [2, 33, 36].

The requirements for temporal resolution depend on the vessel of interest: high temporal resolution is needed for vessels with pulsatile flow like the aorta and visceral arteries. Constant flow in the portal venous system and some systemic veins can be sufficiently measured with lower temporal resolution. Arterial measurements should be obtained with a temporal resolution below 40 ms [2] if possible. Typically reported temporal resolutions for exams focusing on the portal venous system range between 30 to 70 ms, corresponding to 9 to 15 time frames per cardiac cycle, depending on heart rate [6, 7, 9, 12–15, 17, 24, 25, 33–35]. One study even proposed using time-averaged reconstructions for the portal venous system showing more consistent flow quantification and higher visualization quality compared to time-resolved reconstructions [35].

To compensate for breathing motion and to reduce motion artifacts, respiratory gating or compensation should be applied using respiratory bellows or navigator-based strategies. Navigators should be placed at the liver-lung interface or can be placed on the spleen-lung interface, in order to not interfere with the main region of interest. An acceptance window of 50–60% should be used, corresponding to a fixed acceptance window of approximately 6 to 8 mm [6, 9, 37]. Alternatively, an adaptive acceptance window could be set to an acceptance rate of 50% [13, 14, 17, 34, 35]. Acquisition time could be reduced if data could be acquired continuously with motion correction. Indeed, there are promising studies introducing self-navigated techniques for hepatic flow [15] or self-gating respiratory motion-resolved 4D flow MRI in the heart [38]. Respiratory gating is not typically necessary for retroperitoneal vessels in the pelvis due to low breathing induced motion.

The velocity encoding setting (VENC) defines the maximum positive and negative velocity that can be unambiguously measured with phase contrast MRI. The VENC is set prior to the acquisition and should be chosen carefully to match the expected flow velocities: a VENC chosen too low will result in velocity aliasing in the areas with velocities that are higher than the VENC, resulting in false measurements. If the error is not too large, this can be corrected for by post-processing software applying a phase-unwrapping, i.e., anti-aliasing algorithm. In contrast, a VENC chosen too high will result in decreased signal-to-noise ratio (SNR) and velocity-to-noise ratio (VNR) with inaccurate measurements [1, 39]. A useful recommendation is that the ideal VENC should be chosen to be 10% higher than the maximum expected velocity [2]. To capture different velocities in the arterial and venous system simultaneously, an acquisition with multiple VENCs would be preferable. Emerging dual- or multi-VENC acquisitions have been found to have significantly improved visualization quality: Compared to a single-VENC acquisition they present with higher velocity-to-noise ratio, superior internal flow data consistency (conservation of mass) and less noise [40–43]. The main disadvantage of multi-VENC strategies is the increased acquisition time and/or lower temporal resolution, which ultimately limits the accuracy of flow measurements [19].

4D flow MRI can be acquired with or without contrast agents. Post-contrast acquisitions benefit from higher SNR [44]. To fully exploit this benefit, the flip angle should be increased with post-contrast acquisitions [2], such that the Ernst angle is chosen to maximize the spoiled gradient echo signal based on the anticipated T1 value and repetition time. Most sites acquiring 4D flow MRI for research or in clinical routine generally prefer post-contrast acquisitions because of the improved SNR, and the resulting visualization of smaller branch vessels. 4D flow MRI is typically performed after contrast administered for other purpose, or occasionally contrast is administered for the sole purpose of improving 4D flow MRI measurements. One viable off-label alternative to gadolinium-based contrast agents is the use of Ferumoxytol (Feraheme, AMAG, Waltham, MA, USA). It is a superparamagnetic iron oxide agent that is FDA-approved for treatment of renal failure associated anemia. It has favorable MRI properties acting as a blood pool agent [45], and it is gaining increasing acceptable for clinical and research MRI applications [46], including 4D flow MRI [47].

Post-processing and quality control

Since recently, various post-processing software packages for 4D flow MRI research and clinical evaluations are available. Arterys (Arterys Inc, San Francisco, CA, USA), CAAS (PIE Medical Imaging, Maastricht, The Netherlands), cvi42 (Circle Cardiovascular Imaging Inc, Calgary, Canada), Medis Suite MR (Medis Medical Imaging, Leiden, The Netherlands), and suiteHEART (NeoSoft, Pewaukee, USA) have received clearance for clinical use in many countries for basic 4D flow post-processing. Other software packages are dedicated research applications, e.g., FourFlow (Lund University, Sweden), GTFlow (GyroTools, Zurich, Switzerland), and MEVISFlow (Fraunhofer MEVIS, Bremen, Germany).

Post-processing should include correction of background phase offsets due to concomitant gradient fields (Maxwell terms) and eddy currents [2]. Commercial MR systems automatically correct for well-defined concomitant gradient fields in their image reconstruction process. Post-processing software for 4D flow MRI offers offline correction for additional eddy current induced phase inhomogeneities prior to data analysis. Some MR vendors have also implemented a correction for eddy current effects in the reconstruction process for 4D flow MRI at the MR system. Accurate correction strategies are necessary to reduce measurement errors and improve internal consistency [48]. If present, velocity aliasing should be corrected.

Prior to clinical evaluation we recommend quality control of the acquired 4D flow dataset. This includes visual inspection of the source images (phase contrast and magnitude) for signal intensity, noise, artifacts, and velocity aliasing. This should be followed by a quantitative evaluation of internal data consistency, i.e., validation of conservation of mass [48]. Therefore, the inflow and outflow volumes of branching vessels should match (e.g., suprarenal aorta = renal arteries + infrarenal aorta, or superior mesenteric vein + splenic vein = portal vein = right + left portal vein). Alternatively, flow volumes within a vessel region without branching vessels should be consistent when measured at different positions [48]. Typical mean bias of stroke volumes of arterial vessels in the upper abdomen were reported 2–15% [33, 48, 49] with patients presenting with errors in the higher range of the spectrum. For the portal venous system, mean bias in conservation of mass analysis ranged between 3% and 9% [11–13, 33, 35].

Data analysis and relevant parameters

Analysis of 4D flow MRI typically includes qualitative and quantitative parameters. Vessel anatomy can be assessed in a 3D angiogram-derived from complex difference images (Fig. 1b). Flow can be quantified and visualized with time-resolved pathlines and instantaneous streamlines. Streamlines are instantaneously tangent to the velocity vector field and capture the 3D velocity field at a specific temporal phase (Fig. 1d). In pulsatile flow, the velocity field is constantly changing. Therefore, streamlines do not represent the path of a blood cell through the vessel but rather a snapshot of the flow profile at a given time. Pathlines account for the temporal changes of the flow field by following the paths of virtual massless fluid particles through the dynamic velocity field. Pathlines, unlike streamlines, come closest to visualizing the actual path of blood through space and time [2]. The description of secondary

flow patterns, meaning flow patterns that deviate from the main forward stream (e.g., helical or vortical flow) is a typical qualitative parameter of 4D flow MRI analyses [50, 51].

4D flow provides measurements of the velocity (units = m/s) over the entire 3D volume, over multiple time points through the cardiac cycle. Instantaneous flow (ml/s) can be measured in a vessel through contouring its cross section and adding the velocity contributions to flow within the vessel. If contouring is performed in that vessel at all time points over the cardiac cycle, volumetric flow or flow volume (ml/cardiac cycle or ml/min) can be measured by integrating the instantaneous flow measurements over time.

There are many advanced parameters that can be derived from 4D flow MRI data that show promising clinical value [2]. Due to lack of large, multi-center, long-term follow up studies proving their clinical impact, they have not been established in clinical routine yet. Wall shear stress (WSS) describes the viscous shear forces of the flowing blood that act tangentially to the vessel wall and thereby acting on the endothelial cells. Pathological WSS can potentially induce vessel remodeling including development of atherosclerosis or aneurysms [52–57]. A closely associated parameter is the oscillatory shear index (OSI) which describes the oscillation of the WSS vector over time [10, 58]. The pulse wave velocity (PWV), which expresses the speed of the propagation of the systolic pressure pulse in the arterial system, is a marker of arterial stiffness and is a strong predictor of cardiovascular risk [59–65]. Turbulent kinetic energy (TKE) is a marker for the energy content of turbulent flow and an estimate of turbulence-related loss of propulsive energy [66–68]. Moreover, measurement of flow velocities allows for the noninvasive estimation of pressure differences in a continuous vessel by the Navier-Stokes equation. Pressure differences can be used to assess severity of stenoses [69–72].

These measurements can be performed by placing interactive 2D planes in the acquired, time-resolved 3D volume. Additionally, some software options allow a more comprehensive evaluation of the 3D, time-resolved data including the depiction of heat maps, 3D comparison to a healthy volunteer atlas, and analyses of the whole vessel volume along a centerline [55, 73–75]. These advanced applications have largely been used for the thoracic aorta. They have yet to be adapted to evaluate branch abdominal vessels, including the splanchnic and hepatic venous systems. In the future, we anticipate that artificial intelligence technologies will be applied to 4D flow MRI, including improved image quality, accelerated post-processing and workflow, and automatic extraction of the rich quantitative information in each 4D flow dataset. First results of cerebrovascular 4D flow MRI enhanced data using machine learning and computational fluid dynamics simulation data are very promising [76].

In the following sections, we discuss current and emerging applications of 4D flow MRI in the abdomen (Table 3).

Abdominal Applications

Liver

The most frequently analyzed vasculature in the abdomen with 4D flow MRI are the liver vessels, notably the portal venous system. Hemodynamics play an essential role in many

hepatic pathologies. To date, most research is focused on liver cirrhosis, the final stage of advanced liver disease characterized by advanced liver fibrosis, liver failure and portal hypertension.

As cirrhosis progresses, resistance to portal flow increases due to a combination of increased passive resistance at the sinusoidal level from fibrosis and increased dynamic resistance from reduced nitric oxide release, a potent vasodilator that regulates stellate cell and smooth muscle contraction [77]. Further, cirrhotic patients have elevated circulating levels of endogenous vasodilators, leading to systemic hypotension and compensatory increases in cardiac output [78]. This leads to an increase of portal blood flow which is a major contributor to elevated portal pressure. Compensatory, portosystemic collaterals develop from pre-existing anastomoses shunting blood away from the portal vein into the systemic circulation [79] (Fig. 2).

Cirrhosis: diagnosis and grading—A promising approach to diagnose and grade liver cirrhosis with 4D flow MRI is the comparison of fasting and postprandial hemodynamics as proposed by Roldán-Alzate et al [13]. In fasting state, they did not find significant differences in portal flow between patients with mostly mild cirrhosis and healthy volunteers. However, after a meal challenge, they found substantial differences between both cohorts: azygos vein flow increased significantly in cirrhotic patients, but not healthy controls, indicating increased portosystemic shunting volume. Moreover, response to a meal challenge, i.e., increase in flow volumes, was blunted in cirrhotics compared to healthy volunteers. The same was true for the portal vein flow fraction, i.e., flow in the portal vein compared to the total liver blood flow (arterial and portal venous), which increased less in patients than in volunteers. These differences were not statistically significant, probably due to a heterogenous patient cohort with mostly mild cirrhosis. Nonetheless, analyzing the response to a meal challenge could help identify patients with early stages of portal hypertension that cannot be detected with fasting hemodynamic analysis alone.

Flow reversal in the portal vein, superior mesenteric vein, or splenic vein, as well as direct visualization and measurement of collateral flow, e.g., in the paraumbilical collaterals were reported in multiple studies in some patients with cirrhosis [3, 6, 9, 12, 13, 34] (Fig. 3c). These findings are highly specific for portal hypertension.

Cirrhosis: identification of patients with increased risk for variceal bleeding—Approximately 40% of patients with compensated cirrhosis have varices at the time of diagnosis [80, 81]. Gastroesophageal varices (GEV) are the most clinically relevant portosystemic collaterals. GEV are prone to rupture associated with severe bleeding which is the direct cause of death in about 30% of cirrhotic patients [82]. Early detection of GEV at risk for bleeding is of paramount importance to initiate primary prophylaxis [83], that can reduce mortality by 50–70% [84–86]. The American Society for the Study of Liver Diseases (AASLD) and Baveno guidelines recommend initial esophagogastroduodenoscopy (EGD) screening in patients with newly diagnosed cirrhosis [83, 87, 88] with control EGD every 1–3 years [83, 87, 88]. Compliance with this surveillance scheme is poor as EGD is invasive, expensive, and requires sedation. Therefore, the AASLD has identified the development of

non-invasive markers that predict the presence of high-risk varices as a major unmet need in the management of cirrhosis [88].

Early studies with 4D flow MRI show very promising results indicating that this method could become a non-invasive alternative for EGD screening. 4D flow MRI-based identification of high-risk varices focuses on the fact that GEV are mostly supplied by reversed (i.e.: hepatofugal) flow from the left gastric vein. In these cases, blood is drained away from the portal vein via the left gastric vein into the varices and subsequently into the azygos vein (Fig. 2). In this way, portal venous blood is shunted into the systemic circulation bypassing the liver. Taking this mechanism into account, Motosugi et al [34] introduced the non-invasive biomarker "fractional flow change" in the portal vein measured by 4D flow MRI for the detection of GEV at risk for bleeding. Since the left gastric vein often may be too small to be directly identified by 4D flow MRI, Motosugi et al proposed an indirect method to prove the presence of hepatofugal flow: Over the course of the portal vein, several smaller vessels drain into the portal vein resulting in an increased blood flow volume at the portal bifurcation. If some of these tributary vessels, namely the left gastric vein, show hepatofugal flow and drain blood away from the portal vein, there is a decrease in the expected flow between the proximal (PV_{prox}) and distal (PV_{dist}) portal vein. In order not to miss the left gastric vein that can drain into the mesosplenic confluence, it is recommended to measure flow volumes of superior mesenteric vein (SMV) and splenic vein (SV) as a proxy for the proximal portal vein. The fractional flow change can be calculated as follows:

$$\begin{aligned} Fractional\ flow\ change\ in\ portal\ vein &= \frac{PV_{dist} - PV_{prox}}{PV_{prox}} \\ &= \frac{PV_{dist} - (SMV + SV)}{SMV + SV} \end{aligned} \quad [1]$$

where PV_{prox}, PV_{dist}, SMV, and SV are the volumetric flow rates in the proximal and distal portal vein, superior mesenteric vein, and splenic vein, respectively. A fractional flow change below zero indicates hepatofugal flow in branches of the portal vein as more blood enters the portal vein at the confluence than arrives at the liver hilum (Fig. 3). This method indirectly measures blood that is shunted away from the liver. When compared to EGD, a negative fractional flow change identified high-risk varices with high sensitivity (100%) and specificity (94%) in seven out of 23 patients with cirrhosis. Moreover, increased azygos flow greater than 0.1 L/min was a secondary predictor of high-risk varices (sensitivity 100%, specificity 62%) [34]. Importantly, accurate measurement of the fractional flow change in the portal vein should account for anatomical variants, e.g., when the left gastric vein drains into the splenic vein and will therefore need to be adapted to the individual's anatomy. If confirmed in larger studies, 4D flow MRI could potentially reduce the need for purely diagnostic EGD procedures and increase compliance of surveillance of gastroesophageal varices through access to an alternative non-invasive method.

Cirrhosis: identification of patients with severe hypersplenism—Portal hypertension can induce hypertrophy of the spleen resulting in increased pooling and consumption of platelets and leukocytes. This can subsequently lead to thrombocytopenia and leukopenia which are independent risk factors for variceal bleeding, spontaneous

bacterial peritonitis, and death in this patient cohort [89–91]. In a cohort of 29 patients with portal hypertension, Keller et al [19] established the splenic flow index incorporating the splenic volume derived from anatomical MRI images and the blood flow in splenic artery and vein, as well as the percentage of shunted portal flow derived from 4D flow MRI data normalized to body surface area. Applying this index to 10 patients with portal hypertension, they were able to detect severe hypersplenism confirmed by laboratory tests with 100% sensitivity and 100% specificity. In patients with thrombocytopenia, the identification of portal hypertension as the cause of hypersplenism could potentially inform therapeutic decisions such as splenectomy or splenic artery embolization.

Cirrhosis: evaluation of transjugular intrahepatic portosystemic shunts (TIPS)
—In patients with portal hypertension where conservative measures have failed to control ascites and variceal hemorrhage a transjugular intrahepatic portosystemic shunt (TIPS) can be implanted. TIPS is an invasive procedure where a portosystemic shunt is percutaneously placed, typically connecting the right hepatic vein to the right portal vein. Consequently, it diverts blood from the portal system directly into the liver veins and inferior vena cava circumventing the liver [92, 93]. Complications of TIPS include in-stent stenosis or thrombosis leading to decreased shunting volume, as well as detection of increased shunting volume, e.g., due to mis-sizing of the stent and leading to hepatic encephalopathy due to increased levels of ammonia [94]. These complications can be evaluated through measurements of shunt volumetric flow and velocities detected by 4D flow MRI [95]. Pre- and post-interventional analysis should reveal a significant increase in flow volume and peak velocity in the portal venous system after the procedure [17, 37, 96] (Fig. 4). For further evaluation, the shunt fraction, defined as the ratio between flow volume in the TIPS in relation to the portal vein, could give information about the functionality of the TIPS [17]. In another study, the simultaneous presence of both visually detected focal turbulence and pathologically de- or increased peak velocities (>190cm/s or <90cm/s [97]) was 100% sensitive and 100% specific for shunt dysfunction that was confirmed in three of sixteen patients with TIPS [37].

Surgical planning and follow up—4D flow MRI can be used for surgical planning and could help finding the best surgical strategy and predicting outcome. Rutkowski et al [98] proposed a workflow including pre-operative 4D flow MRI, virtual surgery, computational fluid dynamics (CFD) simulations and in vitro models for living liver donors. In partial liver transplantation, both the liver donors and the graft recipients are at risk for post-surgical portal hypertension and tissue damage: Since the central vasculature cannot regenerate, the entire portal blood flows through the post-operatively smaller vascular bed, inevitably leading to higher resistance [99]. Accounting for the ability of the portal venous system to dilate after a meal into account, the authors were able to predict postoperative hemodynamics.

Another study analyzed the added value of 4D flow MRI in predicting the effect of hepatic vessel flow on microwave ablation volumes in a healthy porcine liver model. Although they did not find a significant correlation, accounting for flow in the hepatic veins to the hepatic vein size improved the accuracy of the ablation volume regression model [100].

Aorta

Typical pathologies of the abdominal aorta where 4D flow MRI can give valuable information include aneurysms, dissections, and atherosclerosis. In abdominal aortic aneurysms and dissections, the ultimate application of 4D flow MRI would be the risk assessment for progression and rupture. The first step into this direction is to characterize flow patterns and measurements in these pathologies rigorously. Long-term follow up studies will then be needed to correlate patient outcome with specific 4D flow MRI-derived parameters. Currently, most research groups are focusing on the characterization of pathological hemodynamics.

Aortic dissections: prediction of progression and rupture risk—Liu et al [101] described hemodynamics in the true and false lumen of type B dissection in the distal thoracic and abdominal aorta (Fig. 5). For example, they found that the larger the intimal entry's size, the lower the velocity and flow rate in the true lumen. Conversely, larger entry size correlated with higher average through-plane velocity, average net flow, and peak flow in the false lumen. These parameters should be evaluated as metrics predicting the risk of rupture from aneurysmal dilatation of abdominal aortic dissections, in long-term follow up studies. Burris et al reported early studies in the thoracic aorta of patients with type B aortic dissection [102]. These investigators found that the false lumen ejection fraction, as defined as the proportion between retrograde and antegrade flow measured at the dominant entry tear, was an independent predictor of growth rate. However, they acquired the MRI several years after the initial dissection and calculated the growth rate of the aorta compared to a baseline CT study. Larger follow up studies with baseline 4D flow MRI to determine the impact of the described flow changes on progression are needed.

Characterization of hemodynamics in abdominal aortic aneurysms—Takehara et al [10] found increased vortical and helical flow in infrarenal abdominal aneurysms compared to the undilated suprarenal aorta in 18 subjects. Pathological flow patterns were accompanied by decreased velocity, decreased WSS and increased OSI in the aneurysms [10, 26]. The constant exposure of the aneurysm wall to atherogenic stimuli could further promote aneurysm progression. Interestingly, Sughimoto et al [103] found elevated OSI in healthy volunteers in the infrarenal abdominal aorta where abdominal aortic aneurysms commonly occur.

Identifying endoleaks and stenoses after endovascular aortic repair and predicting aneurysm sac expansion—Studies have shown first promising results for the application of 4D flow MRI in the evaluation of endovascular aortic repair (EVAR) [104, 105], (Fig. 6). 4D flow MRI was reported to be more sensitive in detecting endoleaks after EVAR than CTA. In contrast to CTA, 4D flow MRI allowed the differentiation between type II endoleaks from branch vessels into those with a single vessel or with multiple vessels involved. In addition to endoleaks that were already detected by digital subtraction angiography or CTA, 4D flow MRI indicated additional, concomitant endoleaks in 7/18 patients [106]. However, since these additional endoleaks could only be detected by 4D flow MRI, the rate of false positives remains unclear. The same group examined 107 patients seven days after EVAR with nitinol-based stent grafts with 4D flow MRI and CTA and

found 39 patients with type II endoleaks. After a one-year follow-up, 7/28 patients with type II endoleaks had sac expansion which was associated with a significantly higher "amplitude of dynamics" of the blood flow at the initial MRI exam. They defined the blood flow "amplitude of dynamics" as the total of the absolute inflow and outflow volume measured by 4D flow MRI. With a threshold of 3.75 ml/min absolute inflow and outflow volume per aneurysm sac, they found a positive predictive value of 86% and a negative predictive value of 76% for sac expansion [107].

Another group measured a 4D flow MRI-derived pressure gradient across a narrowed segment of an endoprosthesis to determine the clinical significance of the stenosis. The results were confirmed by invasive pressure measurements [108].

Assessment of cardiovascular risk—Wentland et al [63] evaluated PWV using 4D flow MRI in the abdominal aorta in an animal model in swine with familial hypercholesterolemia against pressure probes. They found that PWV significantly increased in swine with atherosclerotic lesions compared to those without atherosclerotic lesions in the abdominal aorta. This underlines the value of 4D flow MRI-derived PWV as a biomarker for cardiovascular risk assessment.

Kidneys

Detection and grading of renal artery stenosis—4D flow MRI can be used to evaluate renal artery stenosis associated with hypertension, fibromuscular dysplasia, renal insufficiency, cardiac destabilization, or renal transplant dysfunction. Anatomical imaging is sufficient to identify hemodynamically significant stenosis defined as at least 70% luminal reduction. Historically, determination of the hemodynamic significance of moderate stenoses of 50–70% requires additional hemodynamic tests such as invasive intraarterial pressure measurements or duplex ultrasonography [109, 110]. In these cases, a transstenotic mean gradient of 10 mmHg or a systolic gradient of 20mmHg indicate a hemodynamically significant stenosis. However, intraarterial pressure measurements are invasive and ultrasound is strongly dependent on operator skills, patient's body habitus, and presence of bowel gas. Identifying and grading renal artery stenosis based on both anatomical and hemodynamic parameters is possible with 4D flow MRI as proven in initial studies.

Francois et al [16] introduced 1mm isotropic, radial 4D flow MRI-derived complex difference MRA without contrast agent administration as an adequate alternative to contrast-enhanced MRA, with comparable results regarding the visualization and identification of renal artery stenosis (Fig. 7).

Importantly, Bley et al confirmed that 4D flow MRI measurements of the transstenotic pressure gradient produced highly accurate results in stenoses between 0 – 87% compared to endovascular pressure measurements in a swine model of renal artery stenosis [72]. The measurement failed in 5/24 cases with stenoses between 75%–100% since the residual lumen was too small. However, in these cases the transstenotic pressure gradient was not relevant since they already were defined as severe stenoses based on high luminal reduction. The non-invasive assessment of renal artery stenosis without ionizing radiation or contrast

media is of particular interest in children, for example, as described in a case report by Ishikawa et al [111].

Assessment of kidney transplants—Another promising application of 4D flow MRI is the assessment of flow after kidney transplantation. Motoyama et al [112] confirmed that depiction of anatomy and flow measurements not only in the renal artery but also in segmental and interlobar arteries in renal transplants was feasible with radial 4D flow MRI without the need for contrast agents, correlating well with both CTA and ultrasound. Bane et al [18] examined renal transplant patients with stable function and with chronic renal allograft dysfunction focusing on flow rate in the transplant arteries and veins. They demonstrated good diagnostic performance of renal artery and vein flow with significantly reduced values in dysfunctional allografts compared to functional grafts. Moreover, flow in the renal artery correlated with histopathologic interstitial fibrosis score and moderately with estimated glomerular filtration rate (eGFR). It remains unclear whether these distinct flow changes are the cause or the consequence of allograft dysfunction. As no vascular stenosis or occlusion was found, the latter seems more likely. Long-term follow up studies are necessary to evaluate possible predictive flow parameters for graft dysfunction.

Surgical planning and surveillance of medical treatment—To guide surgical treatment in patients with inconclusive conventional imaging, 4D flow MRI can offer valuable information on residual flow in vessels with intravascular tumor growth (Fig. 8). Interestingly, results of medical treatment can also be surveilled with 4d Flow MRI. Takayama et al [113] proposed monitoring of neoadjuvant sunitinib treatment aimed at reducing pathologic angiogenesis in a patient with renal cell carcinoma. In a single patient, they described initial reduction of flow rate in the main tumor feeding artery with redistribution of flow to the healthy parts of the kidney indicating treatment response. When sunitinib treatment needed to be reduced due to side effects, these flow findings reversed. The authors interpreted this as failing response to neoadjuvant treatment and the patient was operated.

Gastrointestinal Tract

Diagnosis of chronic mesenteric ischemia—Atherosclerotic stenosis of the celiac trunk or the superior mesenteric artery are relatively common in older patients while functional stenosis under the median arcuate ligament (median arcuate ligament syndrome, MALS) is more prevalent in younger patients [114]. Due to a high degree of collateralization in the gastrointestinal system, chronic ischemia and associated symptoms are relatively rare. Diagnosis of chronic mesenteric ischemia is challenging, and imaging includes anatomical cross-sectional imaging (CT, MRI) without functional information. As in other vascular territories, sonography offers both anatomical and hemodynamic information but can often be of limited value under suboptimal examination conditions [115]. The European guidelines on chronic mesenteric ischemia emphasize that "a sensitive and specific (functional) test is needed to help detect ischemia and identify chronic mesenteric ischemia patients" and noted that this "should be considered an important research topic" [114].

Siedek et al [49] confirmed the feasibility of 4D flow MRI in the celiac trunk and the superior mesenteric artery in healthy volunteers and patients with confirmed low- and mid-grade stenosis of either vessel. As expected in stenotic vessels, they found higher velocities, lower peak flow and stroke volume, as well as higher average wall shear stress magnitude in patients with mid-grade stenoses. They demonstrated that the severity of the stenosis agreed well between CT and complex difference visualization of the 4D flow MRI. This underlines the valuable combination of hemodynamic and anatomical evaluation feasible with 4D flow MRI.

Roberts et al [14] and Hall Barrientos et al [22] reported very promising results that 4D flow MRI may be an effective solution to the unmet need of diagnosing chronic mesenteric ischemia non-invasively with anatomical and hemodynamic imaging. In patients with chronic mesenteric ischemia, they found no significant flow increase in the superior mesenteric artery and vein or the portal vein after a meal challenge (Fig. 9). In contrast, healthy volunteers, and patients with initially suspected but finally excluded chronic mesenteric ischemia presented with a significant increase in postprandial blood flow in these vessels after a meal challenge (e.g., post-prandial increase in flow in the superior mesenteric artery in healthy volunteers: 99±81%, compared to patients with chronic mesenteric ischemia: 25±30%, [14]). In future studies, it may be interesting to include the inferior mesenteric artery in the volume of interest to capture possible mechanisms of flow collateralization. Since ranges of flow increase overlapped between the groups, larger studies are necessary to define possible cut-off values for clinical diagnosis.

Another interesting application of 4D flow MRI could be the characterization of celiac trunk stenosis by the median arcuate ligament. Initial cases suggest that a meal challenge could determine the relevance of the stenosis in inconclusive cases (Fig. 10).

Placenta and Uterus

Hemodynamics in the uterine arteries is essential for adequate perfusion of the placenta and ultimately the fetus. Ultrasound-derived total uterine artery blood volume flow rate in the first trimester has been shown to correlate with birth weight and gestational age at delivery [116]. Many pregnancy disorders such as preeclampsia and fetal growth restriction are characterized by arterial dysfunction. Since vascular anatomy is complex, and vessels are small and tortuous, ultrasound and 2D flow MRI measurements are challenging. Further, gadolinium-based contrast agents in the first trimester of pregnancy are associated with an increased risk for rheumatological, inflammatory, or infiltrative skin conditions of the child, and for stillbirth or neonatal death [117]. For this reason, 4D flow MRI studies during pregnancy should be conducted without administration of gadolinium-based contrast agents. One viable off-label alternative is the use of ferumoxytol-enhanced 4D flow MRI.

Prediction of pregnancy complications—In preclinical studies in non-human primates, MacDonald et al [118] demonstrated the feasibility of ferumoxytol-enhanced 4D flow MRI measurements of uteroplacental flow, with good consistency and repeatability. Hwuang et al [119] further demonstrated feasibility of uterine artery anatomy characterization as well as flow and velocity measurements including pulsatility and

resistivity indices in 44 pregnant human subjects in the second and third trimester without contrast administration. In a follow-up study of 74 pregnant women, they found a significantly lower uterine artery blood flow rate in the second and third trimester in 18 subjects that later developed pregnancy complications (either preeclampsia and/or small for gestational age) compared to uncomplicated pregnancies and deliveries. Moreover, MRI- and ultrasound-derived uterine artery pulsatility indices, originally established for ultrasound, were significantly increased in subjects with pregnancy complications [120]. In the future, 4D flow MRI could become a reproducible, non-invasive marker for blood flow analysis in pregnancy in areas of anatomy not accessible by ultrasound and with the potential to early detect individuals with increased risk for complications (Fig. 11).

Conclusion

4D flow MRI allows the comprehensive assessment of the complex abdominal vasculature and better understanding of its pathologies. The main advantage over other imaging methods is the simultaneous, objective assessment of both, hemodynamics and morphology in a large imaging volume. Data can be retrospectively analyzed applying advanced post-processing software that allow qualitative assessment as well as quantitative analyses of standard and advanced hemodynamic metrics.

Potential areas of use range from the pure diagnosis of pathologies to comprehensive risk-stratification, including prediction of outcome. Promising examples of non-invasive diagnosis and grading of pathologies include cirrhosis, vessel stenoses, and surveillance of medical and surgical treatment. Non-invasive risk stratification using 4D flow MRI for early detection of patients with liver cirrhosis at high risk for variceal bleeding as well as the prediction of progression of aneurysms, dissections and endoleaks have tremendous potential to impact clinical care.

To date, 4D flow MRI has been used clinically only in some specialized centers. Where available, physicians and surgeons frequently request 4D flow imaging to help them understand disease states and treatment options for their individual patients. To pave the way for widespread adoption into clinical routine, continued technical development as well as longitudinal, multi-center follow up studies are needed to demonstrate the clinical utility of the method in larger cohorts. Implementation will be further facilitated by shorter acquisition times and faster, automated post-processing algorithms.

Acknowledgements

References

1. Markl M, Frydrychowicz A, Kozerke S, Hope M, Wieben O (2012) 4D flow MRI. J Magn Reson Imaging 36(5): 1015–1036. 10.1002/jmri.23632 [PubMed: 23090914]

2. Dyverfeldt P, Bissell M, Barker AJ, Bolger AF, Carlhall CJ, Ebbers T, Francios CJ, Frydrychowicz A, Geiger J, Giese D, Hope MD, Kilner PJ, Kozerke S, Myerson S, Neubauer S, Wieben O, Markl M (2015) 4D flow cardiovascular magnetic resonance consensus statement. J Cardiovasc Magn Reson 17(1): 72. 10.1186/s12968-015-0174-5 [PubMed: 26257141]

3. Roldan-Alzate A, Francois CJ, Wieben O, Reeder SB (2016) Emerging Applications of Abdominal 4D Flow MRI. AJR. American journal of roentgenology 207(1): 58–66. 10.2214/AJR.15.15995 [PubMed: 27187681]

4. Riedel C, Lenz A, Fischer L, Li J, Piecha F, Kluwe J, Adam G, Bannas P (2021) Abdominal Applications of 4D Flow MRI. RoFo : Fortschritte auf dem Gebiete der Rontgenstrahlen und der Nuklearmedizin 193(4): 388–398. 10.1055/a-1271-7405 [PubMed: 33264806]

5. Frydrychowicz A, Roldan-Alzate A, Winslow E, Consigny D, Campo CA, Motosugi U, Johnson KM, Wieben O, Reeder SB (2017) Comparison of radial 4D Flow-MRI with perivascular ultrasound to quantify blood flow in the abdomen and introduction of a porcine model of pre-hepatic portal hypertension. Eur Radiol 27(12): 5316–5324. 10.1007/s00330-017-4862-4 [PubMed: 28656461]

6. Stankovic Z, Csatari Z, Deibert P, Euringer W, Blanke P, Kreisel W, Abdullah Zadeh Z, Kallfass F, Langer M, Markl M (2012) Normal and altered three-dimensional portal venous hemodynamics in patients with liver cirrhosis. Radiology 262(3): 862–873. 10.1148/radiol.11110127 [PubMed: 22357888]

7. Stankovic Z, Csatari Z, Deibert P, Euringer W, Jung B, Kreisel W, Geiger J, Russe MF, Langer M, Markl M (2013) A feasibility study to evaluate splanchnic arterial and venous hemodynamics by flow-sensitive 4D MRI compared with Doppler ultrasound in patients with cirrhosis and controls. European journal of gastroenterology & hepatology 25(6): 669–675. 10.1097/MEG.0b013e32835e1297 [PubMed: 23411868]

8. Wentland AL, Grist TM, Wieben O (2013) Repeatability and internal consistency of abdominal 2D and 4D phase contrast MR flow measurements. Acad Radiol 20(6): 699–704. 10.1016/j.acra.2012.12.019 [PubMed: 23510798]

9. Stankovic Z, Frydrychowicz A, Csatari Z, Panther E, Deibert P, Euringer W, Kreisel W, Russe M, Bauer S, Langer M, Markl M (2010) MR-based visualization and quantification of three-dimensional flow characteristics in the portal venous system. J Magn Reson Imaging 32(2): 466–475. 10.1002/jmri.22248 [PubMed: 20677279]

10. Takehara Y, Isoda H, Takahashi M, Unno N, Shiiya N, Ushio T, Goshima S, Naganawa S, Alley M, Wakayama T, Nozaki A (2020) Abnormal Flow Dynamics Result in Low Wall Shear Stress and High Oscillatory Shear Index in Abdominal Aortic Dilatation: Initial in vivo Assessment with 4D-flow MRI. Magn Reson Med Sci 19(3): 235–246. 10.2463/mrms.mp.2019-0188 [PubMed: 32655086]

11. Stankovic Z, Jung B, Collins J, Russe MF, Carr J, Euringer W, Stehlin L, Csatari Z, Strohm PC, Langer M, Markl M (2014) Reproducibility study of four-dimensional flow MRI of arterial and portal venous liver hemodynamics: influence of spatio-temporal resolution. Magn Reson Med 72(2): 477–484. 10.1002/mrm.24939 [PubMed: 24018798]

12. Roldan-Alzate A, Frydrychowicz A, Niespodzany E, Landgraf BR, Johnson KM, Wieben O, Reeder SB (2013) In vivo validation of 4D flow MRI for assessing the hemodynamics of portal hypertension. J Magn Reson Imaging 37(5): 1100–1108. 10.1002/jmri.23906 [PubMed: 23148034]

13. Roldan-Alzate A, Frydrychowicz A, Said A, Johnson KM, Francois CJ, Wieben O, Reeder SB (2015) Impaired regulation of portal venous flow in response to a meal challenge as quantified by 4D flow MRI. J Magn Reson Imaging 42(4): 1009–1017. 10.1002/jmri.24886 [PubMed: 25772828]

14. Roberts GS, Francois CJ, Starekova J, Roldan-Alzate A, Wieben O (2021) Non-invasive assessment of mesenteric hemodynamics in patients with suspected chronic mesenteric ischemia using 4D flow MRI. Abdom Radiol (NY). 10.1007/s00261-020-02900-0

15. Brunsing RL, Brown D, Almahoud H, Kono Y, Loomba R, Vodkin I, Sirlin CB, Alley MT, Vasanawala SS, Hsiao A (2021) Quantification of the Hemodynamic Changes of Cirrhosis with Free-Breathing Self-Navigated MRI. J Magn Reson Imaging 53(5): 1410–1421. 10.1002/jmri.27488 [PubMed: 33594733]

16. Francois CJ, Lum DP, Johnson KM, Landgraf BR, Bley TA, Reeder SB, Schiebler ML, Grist TM, Wieben O (2011) Renal arteries: isotropic, high-spatial-resolution, unenhanced MR angiography with three-dimensional radial phase contrast. Radiology 258(1): 254–260. 10.1148/radiol.10100443 [PubMed: 20980449]

17. Bannas P, Roldan-Alzate A, Johnson KM, Woods MA, Ozkan O, Motosugi U, Wieben O, Reeder SB, Kramer H (2016) Longitudinal Monitoring of Hepatic Blood Flow before and after TIPS by Using 4D-Flow MR Imaging. Radiology 281(2): 574–582. 10.1148/radiol.2016152247 [PubMed: 27171019]

18. Bane O, Said D, Weiss A, Stocker D, Kennedy P, Hectors SJ, Khaim R, Salem F, Delaney V, Menon MC, Markl M, Lewis S, Taouli B (2021) 4D flow MRI for the assessment of renal transplant dysfunction: initial results. Eur Radiol 31(2): 909–919. 10.1007/s00330-020-07208-7 [PubMed: 32870395]

19. Keller EJ, Kulik L, Stankovic Z, Lewandowski RJ, Salem R, Carr JC, Schnell S, Markl M, Collins JD (2017) JOURNAL CLUB: Four-Dimensional Flow MRI-Based Splenic Flow Index for Predicting Cirrhosis-Associated Hypersplenism. AJR. American journal of roentgenology 209(1): 46–54. 10.2214/AJR.16.17620 [PubMed: 28463524]

20. Someya N, Endo MY, Fukuba Y, Hayashi N (2008) Blood flow responses in celiac and superior mesenteric arteries in the initial phase of digestion. American journal of physiology. Regulatory, integrative and comparative physiology 294(6): R1790–1796. 10.1152/ajpregu.00553.2007 [PubMed: 18385466]

21. Sidery MB, Macdonald IA, Blackshaw PE (1994) Superior mesenteric artery blood flow and gastric emptying in humans and the differential effects of high fat and high carbohydrate meals. Gut 35(2): 186–190. 10.1136/gut.35.2.186 [PubMed: 8307468]

22. Hall Barrientos P, Knight K, Black D, Vesey A, Roditi G (2021) A pilot study investigating the use of 4D flow MRI for the assessment of splanchnic flow in patients suspected of mesenteric ischaemia. Sci Rep 11(1): 5914. 10.1038/s41598-021-85315-1 [PubMed: 33723302]

23. Nayak KS, Nielsen JF, Bernstein MA, Markl M, P DG, R MB, Saloner D, Lorenz C, Wen H, B SH, Epstein FH, J NO, Raman SV (2015) Cardiovascular magnetic resonance phase contrast imaging. J Cardiovasc Magn Reson 17(1): 71. 10.1186/s12968-015-0172-7 [PubMed: 26254979]

24. Bane O, Peti S, Wagner M, Hectors S, Dyvorne H, Markl M, Taouli B (2019) Hemodynamic measurements with an abdominal 4D flow MRI sequence with spiral sampling and compressed sensing in patients with chronic liver disease. J Magn Reson Imaging 49(4): 994–1005. 10.1002/jmri.26305 [PubMed: 30318674]

25. Dyvorne H, Knight-Greenfield A, Jajamovich G, Besa C, Cui Y, Stalder A, Markl M, Taouli B (2015) Abdominal 4D flow MR imaging in a breath hold: combination of spiral sampling and dynamic compressed sensing for highly accelerated acquisition. Radiology 275(1): 245–254. 10.1148/radiol.14140973 [PubMed: 25325326]

26. Ziegler M, Welander M, Lantz J, Lindenberger M, Bjarnegard N, Karlsson M, Ebbers T, Lanne T, Dyverfeldt P (2019) Visualizing and quantifying flow stasis in abdominal aortic aneurysms in men using 4D flow MRI. Magn Reson Imaging 57: 103–110. 10.1016/j.mri.2018.11.003 [PubMed: 30445146]

27. Sekine T, Amano Y, Takagi R, Matsumura Y, Murai Y, Kumita S (2014) Feasibility of 4D Flow MR Imaging of the Brain with Either Cartesian y-z Radial Sampling or k-t SENSE: Comparison with 4D Flow MR Imaging using SENSE. Magnetic Resonance in Medical Sciences advpub. 10.2463/mrms.2013-0008

28. Stankovic Z, Fink J, Collins JD, Semaan E, Russe MF, Carr JC, Markl M, Langer M, Jung B (2015) K-t GRAPPA-accelerated 4D flow MRI of liver hemodynamics: influence of different acceleration factors on qualitative and quantitative assessment of blood flow. MAGMA 28(2): 149–159. 10.1007/s10334-014-0456-1 [PubMed: 25099493]

29. Neuhaus E, Weiss K, Bastkowski R, Koopmann J, Maintz D, Giese D (2019) Accelerated aortic 4D flow cardiovascular magnetic resonance using compressed sensing: applicability, validation and

clinical integration. J Cardiovasc Magn Reson 21(1): 65. 10.1186/s12968-019-0573-0 [PubMed: 31638997]

30. Ma LE, Markl M, Chow K, Huh H, Forman C, Vali A, Greiser A, Carr J, Schnell S, Barker AJ, Jin N (2019) Aortic 4D flow MRI in 2 minutes using compressed sensing, respiratory controlled adaptive k-space reordering, and inline reconstruction. Magn Reson Med 81(6): 3675–3690. 10.1002/mrm.27684 [PubMed: 30803006]

31. Glover GH, Pauly JM (1992) Projection reconstruction techniques for reduction of motion effects in MRI. Magn Reson Med 28(2): 275–289. 10.1002/mrm.1910280209 [PubMed: 1461126]

32. Anderson AG 3rd, Velikina J, Block W, Wieben O, Samsonov A (2013) Adaptive retrospective correction of motion artifacts in cranial MRI with multicoil three-dimensional radial acquisitions. Magn Reson Med 69(4): 1094–1103. 10.1002/mrm.24348 [PubMed: 22760728]

33. Keller EJ, Collins JD, Rigsby C, Carr JC, Markl M, Schnell S (2017) Superior Abdominal 4D Flow MRI Data Consistency with Adjusted Preprocessing Workflow and Noncontrast Acquisitions. Acad Radiol 24(3): 350–358. 10.1016/j.acra.2016.10.007 [PubMed: 27940231]

34. Motosugi U, Roldan-Alzate A, Bannas P, Said A, Kelly S, Zea R, Wieben O, Reeder SB (2019) Four-dimensional Flow MRI as a Marker for Risk Stratification of Gastroesophageal Varices in Patients with Liver Cirrhosis. Radiology 290(1): 101–107. 10.1148/radiol.2018180230 [PubMed: 30325278]

35. Landgraf BR, Johnson KM, Roldan-Alzate A, Francois CJ, Wieben O, Reeder SB (2014) Effect of temporal resolution on 4D flow MRI in the portal circulation. J Magn Reson Imaging 39(4): 819–826. 10.1002/jmri.24233 [PubMed: 24395121]

36. Parekh K, Markl M, Rose M, Schnell S, Popescu A, Rigsby CK (2017) 4D flow MR imaging of the portal venous system: a feasibility study in children. Eur Radiol 27(2): 832–840. 10.1007/s00330-016-4396-1 [PubMed: 27193778]

37. Owen JW, Saad NE, Foster G, Fowler KJ (2018) The Feasibility of Using Volumetric Phase-Contrast MR Imaging (4D Flow) to Assess for Transjugular Intrahepatic Portosystemic Shunt Dysfunction. Journal of vascular and interventional radiology : JVIR 29(12): 1717–1724. 10.1016/j.jvir.2018.07.022 [PubMed: 30396843]

38. Ma LE, Yerly J, Piccini D, Di Sopra L, Roy CW, Carr JC, Rigsby CK, Kim D, Stuber M, Markl M (2020) 5D Flow MRI: A Fully Self-gated, Free-running Framework for Cardiac and Respiratory Motion-resolved 3D Hemodynamics. Radiol Cardiothorac Imaging 2(6): e200219. 10.1148/ryct.2020200219 [PubMed: 33385164]

39. Nayak KS, Nielsen J-F, Bernstein MA, Markl M, D. Gatehouse P, M. Botnar R, Saloner D, Lorenz C, Wen H, S. Hu B, Epstein FH, N. Oshinski J, Raman SV (2015) Cardiovascular magnetic resonance phase contrast imaging. Journal of Cardiovascular Magnetic Resonance 17(1): 71. 10.1186/s12968-015-0172-7 [PubMed: 26254979]

40. Ha H, Kim GB, Kweon J, Kim YH, Kim N, Yang DH, Lee SJ (2016) Multi-VENC acquisition of four-dimensional phase-contrast MRI to improve precision of velocity field measurement. Magn Reson Med 75(5): 1909–1919. 10.1002/mrm.25715 [PubMed: 26059014]

41. Schnell S, Ansari SA, Wu C, Garcia J, Murphy IG, Rahman OA, Rahsepar AA, Aristova M, Collins JD, Carr JC, Markl M (2017) Accelerated dual-venc 4D flow MRI for neurovascular applications. J Magn Reson Imaging 46(1): 102–114. 10.1002/jmri.25595 [PubMed: 28152256]

42. Kroeger JR, Pavesio FC, Morsdorf R, Weiss K, Bunck AC, Baessler B, Maintz D, Giese D (2021) Velocity quantification in 44 healthy volunteers using accelerated multi-VENC 4D flow CMR. Eur J Radiol 137: 109570. 10.1016/j.ejrad.2021.109570 [PubMed: 33596498]

43. Moersdorf R, Treutlein M, Kroeger JR, Ruijsink B, Wong J, Maintz D, Weiss K, Bunck AC, Baessler B, Giese D (2019) Precision, reproducibility and applicability of an undersampled multi-venc 4D flow MRI sequence for the assessment of cardiac hemodynamics. Magn Reson Imaging 61: 73–82. 10.1016/j.mri.2019.05.015 [PubMed: 31100318]

44. Bock J, Frydrychowicz A, Stalder AF, Bley TA, Burkhardt H, Hennig J, Markl M (2010) 4D phase contrast MRI at 3 T: effect of standard and blood-pool contrast agents on SNR, PC-MRA, and blood flow visualization. Magn Reson Med 63(2): 330–338. 10.1002/mrm.22199 [PubMed: 20024953]

45. Bashir MR, Bhatti L, Marin D, Nelson RC (2015) Emerging applications for ferumoxytol as a contrast agent in MRI. J Magn Reson Imaging 41(4): 884–898. 10.1002/jmri.24691 [PubMed: 24974785]

46. Vasanawala SS, Nguyen KL, Hope MD, Bridges MD, Hope TA, Reeder SB, Bashir MR (2016) Safety and technique of ferumoxytol administration for MRI. Magn Reson Med 75(5): 2107–2111. 10.1002/mrm.26151 [PubMed: 26890830]

47. Mukai K, Burris NS, Mahadevan VS, Foster ED, Ordovas KG, Hope MD (2018) 4D flow image quality with blood pool contrast: a comparison of gadofosveset trisodium and ferumoxytol. Int J Cardiovasc Imaging 34(2): 273–279. 10.1007/s10554-017-1224-x [PubMed: 28884401]

48. Craiem D, Pascaner AF, Casciaro ME, Gencer U, Alcibar J, Soulat G, Mousseaux E (2019) Automatic correction of background phase offset in 4D-flow of great vessels and of the heart in MRI using a third-order surface model. MAGMA 32(6): 629–642. 10.1007/s10334-019-00765-z [PubMed: 31230182]

49. Siedek F, Giese D, Weiss K, Ekdawi S, Brinkmann S, Schroeder W, Bruns C, Chang DH, Persigehl T, Maintz D, Haneder S (2018) 4D flow MRI for the analysis of celiac trunk and mesenteric artery stenoses. Magn Reson Imaging 53: 52–62. 10.1016/j.mri.2018.06.021 [PubMed: 30008436]

50. Kilner PJ, Yang GZ, Mohiaddin RH, Firmin DN, Longmore DB (1993) Helical and retrograde secondary flow patterns in the aortic arch studied by three-directional magnetic resonance velocity mapping. Circulation 88(5 Pt 1): 2235–2247. 10.1161/01.cir.88.5.2235 [PubMed: 8222118]

51. Oechtering TH, Sieren MM, Hunold P, Hennemuth A, Huellebrand M, Scharfschwerdt M, Richardt D, Sievers HH, Barkhausen J, Frydrychowicz A (2020) Time-resolved 3-dimensional magnetic resonance phase contrast imaging (4D Flow MRI) reveals altered blood flow patterns in the ascending aorta of patients with valve-sparing aortic root replacement. J Thorac Cardiovasc Surg 159(3): 798–810. 10.1016/j.jtcvs.2019.02.127 [PubMed: 31078313]

52. Cheng C, Tempel D, van Haperen R, van der Baan A, Grosveld F, Daemen MJ, Krams R, de Crom R (2006) Atherosclerotic lesion size and vulnerability are determined by patterns of fluid shear stress. Circulation 113(23): 2744–2753. 10.1161/CIRCULATIONAHA.105.590018 [PubMed: 16754802]

53. Davies PF, Spaan JA, Krams R (2005) Shear stress biology of the endothelium. Ann Biomed Eng 33(12): 1714–1718. 10.1007/s10439-005-8774-0 [PubMed: 16389518]

54. Kolipaka A, Illapani VS, Kalra P, Garcia J, Mo X, Markl M, White RD (2017) Quantification and comparison of 4D-flow MRI-derived wall shear stress and MRE-derived wall stiffness of the abdominal aorta. J Magn Reson Imaging 45(3): 771–778. 10.1002/jmri.25445 [PubMed: 27603433]

55. van Ooij P, Potters WV, Collins J, Carr M, Carr J, Malaisrie SC, Fedak PW, McCarthy PM, Markl M, Barker AJ (2015) Characterization of abnormal wall shear stress using 4D flow MRI in human bicuspid aortopathy. Ann Biomed Eng 43(6): 1385–1397. 10.1007/s10439-014-1092-7 [PubMed: 25118671]

56. Sotelo J, Dux-Santoy L, Guala A, Rodriguez-Palomares J, Evangelista A, Sing-Long C, Urbina J, Mura J, Hurtado DE, Uribe S (2018) 3D axial and circumferential wall shear stress from 4D flow MRI data using a finite element method and a laplacian approach. Magn Reson Med 79(5): 2816–2823. 10.1002/mrm.26927 [PubMed: 28980342]

57. van der Palen RLF, Roest AAW, van den Boogaard PJ, de Roos A, Blom NA, Westenberg JJM (2018) Scan-rescan reproducibility of segmental aortic wall shear stress as assessed by phase-specific segmentation with 4D flow MRI in healthy volunteers. MAGMA 31(5): 653–663. 10.1007/s10334-018-0688-6 [PubMed: 29804208]

58. Zimmermann J, Demedts D, Mirzaee H, Ewert P, Stern H, Meierhofer C, Menze B, Hennemuth A (2018) Wall shear stress estimation in the aorta: Impact of wall motion, spatiotemporal resolution, and phase noise. J Magn Reson Imaging. 10.1002/jmri.26007

59. Safar ME, Henry O, Meaume S (2002) Aortic pulse wave velocity: an independent marker of cardiovascular risk. The American journal of geriatric cardiology 11(5): 295–304. [PubMed: 12214167]

60. Willum-Hansen T, Staessen JA, Torp-Pedersen C, Rasmussen S, Thijs L, Ibsen H, Jeppesen J (2006) Prognostic value of aortic pulse wave velocity as index of arterial stiffness in the general

population. Circulation 113(5): 664–670. 10.1161/CIRCULATIONAHA.105.579342 [PubMed: 16461839]

61. Laurent S, Cockcroft J, Van Bortel L, Boutouyrie P, Giannattasio C, Hayoz D, Pannier B, Vlachopoulos C, Wilkinson I, Struijker-Boudier H, European Network for Non-invasive Investigation of Large A (2006) Expert consensus document on arterial stiffness: methodological issues and clinical applications. Eur Heart J 27(21): 2588–2605. 10.1093/eurheartj/ehl254 [PubMed: 17000623]

62. Boutouyrie P, Tropeano AI, Asmar R, Gautier I, Benetos A, Lacolley P, Laurent S (2002) Aortic stiffness is an independent predictor of primary coronary events in hypertensive patients: a longitudinal study. Hypertension 39(1): 10–15. 10.1161/hy0102.099031 [PubMed: 11799071]

63. Wentland AL, Wieben O, Shanmuganayagam D, Krueger CG, Meudt JJ, Consigny D, Rivera L, McBride PE, Reed JD, Grist TM (2015) Measurements of wall shear stress and aortic pulse wave velocity in swine with familial hypercholesterolemia. J Magn Reson Imaging 41(5): 1475–1485. 10.1002/jmri.24681 [PubMed: 24964097]

64. Dyverfeldt P, Ebbers T, Lanne T (2014) Pulse wave velocity with 4D flow MRI: systematic differences and age-related regional vascular stiffness. Magn Reson Imaging 32(10): 1266–1271. 10.1016/j.mri.2014.08.021 [PubMed: 25171817]

65. Markl M, Wallis W, Brendecke S, Simon J, Frydrychowicz A, Harloff A (2010) Estimation of global aortic pulse wave velocity by flow-sensitive 4D MRI. Magn Reson Med 63(6): 1575–1582. 10.1002/mrm.22353 [PubMed: 20512861]

66. Dyverfeldt P, Sigfridsson A, Kvitting JP, Ebbers T (2006) Quantification of intravoxel velocity standard deviation and turbulence intensity by generalizing phase-contrast MRI. Magn Reson Med 56(4): 850–858. 10.1002/mrm.21022 [PubMed: 16958074]

67. Binter C, Knobloch V, Manka R, Sigfridsson A, Kozerke S (2013) Bayesian multipoint velocity encoding for concurrent flow and turbulence mapping. Magn Reson Med 69(5): 1337–1345. 10.1002/mrm.24370 [PubMed: 22700280]

68. Ha H, Ziegler M, Welander M, Bjarnegard N, Carlhall CJ, Lindenberger M, Lanne T, Ebbers T, Dyverfeldt P (2018) Age-Related Vascular Changes Affect Turbulence in Aortic Blood Flow. Front Physiol 9: 36. 10.3389/fphys.2018.00036 [PubMed: 29422871]

69. Yang GZ, Kilner PJ, Wood NB, Underwood SR, Firmin DN (1996) Computation of flow pressure fields from magnetic resonance velocity mapping. Magn Reson Med 36(4): 520–526. 10.1002/mrm.1910360404 [PubMed: 8892202]

70. Tyszka JM, Laidlaw DH, Asa JW, Silverman JM (2000) Three-dimensional, time-resolved (4D) relative pressure mapping using magnetic resonance imaging. J Magn Reson Imaging 12(2): 321–329. 10.1002/1522-2586(200008)12:2<321::aid-jmri15>3.0.co;2-2 [PubMed: 10931596]

71. Ebbers T, Wigstrom L, Bolger AF, Wranne B, Karlsson M (2002) Noninvasive measurement of time-varying three-dimensional relative pressure fields within the human heart. Journal of biomechanical engineering 124(3): 288–293. 10.1115/1.1468866 [PubMed: 12071263]

72. Bley TA, Johnson KM, François CJ (2011) Noninvasive assessment of transstenotic pressure gradients in porcine renal artery stenoses by using vastly undersampled phase-contrast MR angiography. Radiology 261: 266. [PubMed: 21813739]

73. Cibis M, Bustamante M, Eriksson J, Carlhall CJ, Ebbers T (2017) Creating hemodynamic atlases of cardiac 4D flow MRI. J Magn Reson Imaging 46(5): 1389–1399. 10.1002/jmri.25691 [PubMed: 28295788]

74. Garcia J, Barker AJ, Murphy I, Jarvis K, Schnell S, Collins JD, Carr JC, Malaisrie SC, Markl M (2016) Four-dimensional flow magnetic resonance imaging-based characterization of aortic morphometry and haemodynamics: impact of age, aortic diameter, and valve morphology. European heart journal cardiovascular Imaging 17(8): 877–884. 10.1093/ehjci/jev228 [PubMed: 26377908]

75. Gabbert DD, Kheradvar A, Jerosch-Herold M, Oechtering TH, Uebing AS, Kramer H-H, Voges I, Rickers C (2021) MRI-based comprehensive analysis of vascular anatomy and hemodynamics. Cardiovascular diagnosis and therapy.

76. Rutkowski DR, Roldán-Alzate A, Johnson KM (2021) Enhancement of cerebrovascular 4D flow MRI velocity fields using machine learning and computational fluid dynamics simulation data. Scientific reports 11(1): 10240–10240. 10.1038/s41598-021-89636-z [PubMed: 33986368]

77. Bhathal PS, Grossman HJ (1985) Reduction of the increased portal vascular resistance of the isolated perfused cirrhotic rat liver by vasodilators. Journal of hepatology 1(4): 325–337. 10.1016/s0168-8278(85)80770-4 [PubMed: 4056346]

78. Kamath PS, Tyce GM, Miller VM, Edwards BS, Rorie DK (1999) Endothelin-1 modulates intrahepatic resistance in a rat model of noncirrhotic portal hypertension. Hepatology 30(2): 401–407. 10.1002/hep.510300235 [PubMed: 10421647]

79. Garcia-Tsao G, Groszmann RJ, Fisher RL, Conn HO, Atterbury CE, Glickman M (1985) Portal pressure, presence of gastroesophageal varices and variceal bleeding. Hepatology 5(3): 419–424. 10.1002/hep.1840050313 [PubMed: 3873388]

80. Calès P, Desmorat H, Vinel JP, Caucanas JP, Ravaud A, Gerin P, Brouet P, Pascal JP (1990) Incidence of large oesophageal varices in patients with cirrhosis: application to prophylaxis of first bleeding. Gut 31(11): 1298–1302. 10.1136/gut.31.11.1298 [PubMed: 2253916]

81. Chalasani N, Imperiale TF, Ismail A, Sood G, Carey M, Wilcox CM, Madichetty H, Kwo PY, Boyer TD (1999) Predictors of large esophageal varices in patients with cirrhosis. The American journal of gastroenterology 94(11): 3285–3291. 10.1111/j.1572-0241.1999.1539_a.x [PubMed: 10566731]

82. Saunders JB, Walters JR, Davies AP, Paton A (1981) A 20-year prospective study of cirrhosis. British medical journal (Clinical research ed.) 282(6260): 263–266. 10.1136/bmj.282.6260.263 [PubMed: 6779978]

83. Garcia-Tsao G, Abraldes JG, Berzigotti A, Bosch J (2017) Portal hypertensive bleeding in cirrhosis: Risk stratification, diagnosis, and management: 2016 practice guidance by the American Association for the study of liver diseases. Hepatology 65(1): 310–335. 10.1002/hep.28906 [PubMed: 27786365]

84. Bernard B, Lebrec D, Mathurin P, Opolon P, Poynard T (1997) Beta-adrenergic antagonists in the prevention of gastrointestinal rebleeding in patients with cirrhosis: a meta-analysis. Hepatology 25(1): 63–70. 10.1053/jhep.1997.v25.pm0008985266 [PubMed: 8985266]

85. Khuroo MS, Khuroo NS, Farahat KL, Khuroo YS, Sofi AA, Dahab ST (2005) Meta-analysis: endoscopic variceal ligation for primary prophylaxis of oesophageal variceal bleeding. Aliment Pharmacol Ther 21(4): 347–361. 10.1111/j.1365-2036.2005.02346.x [PubMed: 15709985]

86. Pascal JP, Cales P (1987) Propranolol in the prevention of first upper gastrointestinal tract hemorrhage in patients with cirrhosis of the liver and esophageal varices. N Engl J Med 317(14): 856–861. 10.1056/NEJM198710013171403 [PubMed: 3306385]

87. de Franchis R, Baveno VF (2010) Revising consensus in portal hypertension: report of the Baveno V consensus workshop on methodology of diagnosis and therapy in portal hypertension. Journal of hepatology 53(4): 762–768. 10.1016/j.jhep.2010.06.004 [PubMed: 20638742]

88. Garcia-Tsao G, Sanyal AJ, Grace ND, Carey W, Practice Guidelines Committee of the American Association for the Study of Liver D, Practice Parameters Committee of the American College of G (2007) Prevention and management of gastroesophageal varices and variceal hemorrhage in cirrhosis. Hepatology 46(3): 922–938. 10.1002/hep.21907 [PubMed: 17879356]

89. Liangpunsakul S, Ulmer BJ, Chalasani N (2003) Predictors and implications of severe hypersplenism in patients with cirrhosis. The American journal of the medical sciences 326(3): 111–116. 10.1097/00000441-200309000-00001 [PubMed: 14501224]

90. Qamar AA, Grace ND, Groszmann RJ, Garcia-Tsao G, Bosch J, Burroughs AK, Ripoll C, Maurer R, Planas R, Escorsell A, Garcia-Pagan JC, Patch D, Matloff DS, Makuch R, Rendon G, Portal Hypertension Collaborative G (2009) Incidence, prevalence, and clinical significance of abnormal hematologic indices in compensated cirrhosis. Clin Gastroenterol Hepatol 7(6): 689–695. 10.1016/j.cgh.2009.02.021 [PubMed: 19281860]

91. Afdhal N, McHutchison J, Brown R, Jacobson I, Manns M, Poordad F, Weksler B, Esteban R (2008) Thrombocytopenia associated with chronic liver disease. Journal of hepatology 48(6): 1000–1007. 10.1016/j.jhep.2008.03.009 [PubMed: 18433919]

92. Boyer TD, Haskal ZJ, American Association for the Study of Liver D (2010) The Role of Transjugular Intrahepatic Portosystemic Shunt (TIPS) in the Management of Portal Hypertension: update 2009. Hepatology 51(1): 306. 10.1002/hep.23383 [PubMed: 19902484]

93. Allaire M, Walter A, Sutter O, Nahon P, Ganne-Carrie N, Amathieu R, Nault JC (2020) TIPS for management of portal-hypertension-related complications in patients with cirrhosis. Clin Res Hepatol Gastroenterol 44(3): 249–263. 10.1016/j.clinre.2019.09.003 [PubMed: 31662286]

94. Tripathi D, Stanley AJ, Hayes PC, Travis S, Armstrong MJ, Tsochatzis EA, Rowe IA, Roslund N, Ireland H, Lomax M, Leithead JA, Mehrzad H, Aspinall RJ, McDonagh J, Patch D (2020) Transjugular intrahepatic portosystemic stent-shunt in the management of portal hypertension. Gut 69(7): 1173–1192. 10.1136/gutjnl-2019-320221 [PubMed: 32114503]

95. Stankovic Z, Blanke P, Markl M (2012) Usefulness of 4D MRI flow imaging to control TIPS function. The American journal of gastroenterology 107(2): 327–328. 10.1038/ajg.2011.380 [PubMed: 22306955]

96. Stankovic Z, Rossle M, Euringer W, Schultheiss M, Salem R, Barker A, Carr J, Langer M, Markl M, Collins JD (2015) Effect of TIPS placement on portal and splanchnic arterial blood flow in 4-dimensional flow MRI. Eur Radiol 25(9): 2634–2640. 10.1007/s00330-015-3663-x [PubMed: 25850890]

97. McNaughton DA, Abu-Yousef MM (2011) Doppler US of the liver made simple. Radiographics 31(1): 161–188. 10.1148/rg.311105093 [PubMed: 21257940]

98. Rutkowski DR, Reeder SB, Fernandez LA, Roldan-Alzate A (2018) Surgical planning for living donor liver transplant using 4D flow MRI, computational fluid dynamics and in vitro experiments. Comput Methods Biomech Biomed Eng Imaging Vis 6(5): 545–555. 10.1080/21681163.2017.1278619 [PubMed: 30094106]

99. Vasavada BB, Chen CL, Zakaria M (2014) Portal flow is the main predictor of early graft dysfunction regardless of the GRWR status in living donor liver transplantation - a retrospective analysis of 134 patients. Int J Surg 12(2): 177–180. 10.1016/j.ijsu.2013.12.006 [PubMed: 24370677]

100. Chiang J, Loecher M, Moulin K, Meloni MF, Raman SS, McWilliams JP, Ennis DB, Lee EW (2020) 4D Flow MR Imaging to Improve Microwave Ablation Prediction Models: A Feasibility Study in an In Vivo Porcine Liver. Journal of vascular and interventional radiology : JVIR 31(10): 1691–1696 e1691. 10.1016/j.jvir.2019.11.034 [PubMed: 32178944]

101. Liu D, Fan Z, Li Y, Zhang N, Sun Z, An J, Stalder AF, Greiser A, Liu J (2018) Quantitative Study of Abdominal Blood Flow Patterns in Patients with Aortic Dissection by 4-Dimensional Flow MRI. Sci Rep 8(1): 9111. 10.1038/s41598-018-27249-9 [PubMed: 29904131]

102. Burris NS, Nordsletten DA, Sotelo JA, Grogan-Kaylor R, Houben IB, Figueroa CA, Uribe S, Patel HJ (2020) False lumen ejection fraction predicts growth in type B aortic dissection: preliminary results. Eur J Cardiothorac Surg 57(5): 896–903. 10.1093/ejcts/ezz343 [PubMed: 31821480]

103. Sughimoto K, Shimamura Y, Tezuka C, Tsubota K, Liu H, Okumura K, Masuda Y, Haneishi H (2016) Effects of arterial blood flow on walls of the abdominal aorta: distributions of wall shear stress and oscillatory shear index determined by phase-contrast magnetic resonance imaging. Heart and vessels 31(7): 1168–1175. 10.1007/s00380-015-0758-x [PubMed: 26481791]

104. Hope TA, Zarins CK, Herfkens RJ (2009) Initial experience characterizing a type I endoleak from velocity profiles using time-resolved three-dimensional phase-contrast MRI. Journal of vascular surgery 49(6): 1580–1584. 10.1016/j.jvs.2009.01.010 [PubMed: 19223146]

105. Takei Y, Itatani K, Miyazaki S, Shibasaki I, Fukuda H (2019) Four-dimensional flow magnetic resonance imaging analysis before and after thoracic endovascular aortic repair of chronic type B aortic dissection. Interact Cardiovasc Thorac Surg 28(3): 413–420. 10.1093/icvts/ivy271 [PubMed: 30239771]

106. Sakata M, Takehara Y, Katahashi K, Sano M, Inuzuka K, Yamamoto N, Sugiyama M, Sakahara H, Wakayama T, Alley MT, Konno H, Unno N (2016) Hemodynamic Analysis of Endoleaks After Endovascular Abdominal Aortic Aneurysm Repair by Using 4-Dimensional Flow-Sensitive Magnetic Resonance Imaging. Circulation journal : official journal of the Japanese Circulation Society 80(8): 1715–1725. 10.1253/circj.CJ-16-0297 [PubMed: 27357219]

107. Katahashi K, Sano M, Takehara Y, Inuzuka K, Sugiyama M, Alley MT, Takeuchi H, Unno N (2019) Flow dynamics of type II endoleaks can determine sac expansion after endovascular aneurysm repair using four-dimensional flow-sensitive magnetic resonance imaging analysis. Journal of vascular surgery 70(1): 107–116 e101. 10.1016/j.jvs.2018.09.048 [PubMed: 30792053]

108. Salehi Ravesh M, Langguth P, Pfarr JA, Schupp J, Trentmann J, Koktzoglou I, Edelman RR, Graessner J, Greiser A, Hautemann D, Hennemuth A, Both M, Jansen O, Hovener JB, Schafer JP (2019) Non-contrast-enhanced magnetic resonance imaging for visualization and quantification of endovascular aortic prosthesis, their endoleaks and aneurysm sacs at 1.5T. Magn Reson Imaging 60: 164–172. 10.1016/j.mri.2019.05.012 [PubMed: 31075419]

109. Prince M, Tafur JD, White CJ (2019) When and How Should We Revascularize Patients With Atherosclerotic Renal Artery Stenosis? JACC Cardiovasc Interv 12(6): 505–517. 10.1016/j.jcin.2018.10.023 [PubMed: 30898248]

110. Klein AJ, Jaff MR, Gray BH, Aronow HD, Bersin RM, Diaz-Sandoval LJ, Dieter RS, Drachman DE, Feldman DN, Gigliotti OS, Gupta K, Parikh SA, Pinto DS, Shishehbor MH, White CJ (2017) SCAI appropriate use criteria for peripheral arterial interventions: An update. Catheterization and cardiovascular interventions : official journal of the Society for Cardiac Angiography & Interventions 90(4): E90–E110. 10.1002/ccd.27141 [PubMed: 28489285]

111. Ishikawa T, Takehara Y, Yamashita S, Iwashima S, Sugiyama M, Wakayama T, Johnson K, Wieben O, Sakahara H, Ogata T (2015) Hemodynamic assessment in a child with renovascular hypertension using time-resolved three-dimensional cine phase-contrast MRI. J Magn Reson Imaging 41(1): 165–168. 10.1002/jmri.24522 [PubMed: 24615925]

112. Motoyama D, Ishii Y, Takehara Y, Sugiyama M, Yang W, Nasu H, Ushio T, Hirose Y, Ohishi N, Wakayama T, Kabasawa H, Johnson K, Wieben O, Sakahara H, Ozono S (2017) Four-dimensional phase-contrast vastly undersampled isotropic projection reconstruction (4D PC-VIPR) MR evaluation of the renal arteries in transplant recipients: Preliminary results. J Magn Reson Imaging 46(2): 595–603. 10.1002/jmri.25607 [PubMed: 28152259]

113. Takayama T, Takehara Y, Sugiyama M, Sugiyama T, Ishii Y, Johnson KE, Wieben O, Wakayama T, Sakahara H, Ozono S (2014) Use of three-dimensional time-resolved phase-contrast magnetic resonance imaging with vastly undersampled isotropic projection reconstruction to assess renal blood flow in a renal cell carcinoma patient treated with sunitinib: a case report. BMC Res Notes 7(1): 527. 10.1186/1756-0500-7-527 [PubMed: 25125076]

114. Terlouw LG, Moelker A, Abrahamsen J, Acosta S, Bakker OJ, Baumgartner I, Boyer L, Corcos O, van Dijk LJ, Duran M, Geelkerken RH, Illuminati G, Jackson RW, Karkkainen JM, Kolkman JJ, Lonn L, Mazzei MA, Nuzzo A, Pecoraro F, Raupach J, Verhagen HJ, Zech CJ, van Noord D, Bruno MJ (2020) European guidelines on chronic mesenteric ischaemia - joint United European Gastroenterology, European Association for Gastroenterology, Endoscopy and Nutrition, European Society of Gastrointestinal and Abdominal Radiology, Netherlands Association of Hepatogastroenterologists, Hellenic Society of Gastroenterology, Cardiovascular and Interventional Radiological Society of Europe, and Dutch Mesenteric Ischemia Study group clinical guidelines on the diagnosis and treatment of patients with chronic mesenteric ischaemia. United European Gastroenterol J 8(4): 371–395. 10.1177/2050640620916681

115. van Petersen AS, Meerwaldt R, Kolkman JJ, Huisman AB, van der Palen J, van Bockel JH, Zeebregts CJ, Geelkerken RH (2013) The influence of respiration on criteria for transabdominal duplex examination of the splanchnic arteries in patients with suspected chronic splanchnic ischemia. Journal of vascular surgery 57(6): 1603–1611, 1611 e1601–1610. 10.1016/j.jvs.2012.11.120 [PubMed: 23719037]

116. McKelvey A, Pateman K, Balchin I, Peebles DM, Rodeck CH, David AL (2017) Total uterine artery blood volume flow rate in nulliparous women is associated with birth weight and gestational age at delivery. Ultrasound Obstet Gynecol 49(1): 54–60. 10.1002/uog.15917 [PubMed: 26990029]

117. Ray JG, Vermeulen MJ, Bharatha A, Montanera WJ, Park AL (2016) Association Between MRI Exposure During Pregnancy and Fetal and Childhood Outcomes. JAMA : the journal of the American Medical Association 316(9): 952–961. 10.1001/jama.2016.12126 [PubMed: 27599330]

118. Macdonald JA, Corrado PA, Nguyen SM, Johnson KM, Francois CJ, Magness RR, Shah DM, Golos TG, Wieben O (2019) Uteroplacental and Fetal 4D Flow MRI in the Pregnant Rhesus Macaque. J Magn Reson Imaging 49(2): 534–545. 10.1002/jmri.26206 [PubMed: 30102431]

119. Hwuang E, Vidorreta M, Schwartz N, Moon BF, Kochar K, Tisdall MD, Detre JA, Witschey WRT (2019) Assessment of uterine artery geometry and hemodynamics in human pregnancy with 4d flow MRI and its correlation with doppler ultrasound. J Magn Reson Imaging 49(1): 59–68. 10.1002/jmri.26229 [PubMed: 30390347]

120. Hwuang E, Wu PH, Rodriguez-Soto A, Langham M, Wehrli FW, Vidorreta M, Moon B, Kochar K, Parameshwaran S, Koelper N, Tisdall MD, Detre JA, Witschey W, Schwartz N (2020) Cross-modality and in-vivo validation of 4D flow MRI evaluation of uterine artery blood flow in human pregnancy. Ultrasound Obstet Gynecol n/a(n/a). 10.1002/uog.23112

121. Corrado PA, Dinesh MS, Wieben O. 4D Flow MRI of the Uterine and Ovarian Vessels in the 2nd Trimester in Healthy Subjects. in Society of Magnetic Resonance Angiography (SMRA). 2018. Glasgow, Scotland.

Key points for each section

Introduction:

- 4D flow MRI is a phase contrast MRI technique that measures velocities in a three-dimensional volume in three directions, resolved in time, hence "4D".

- 4D flow MRI of the abdomen holds promise for a wide range of clinical applications but is technically challenging.

Technical Aspects:

- Patients should fast at least 5 hours prior to evaluation of the splanchnic circulation.

- Consider acquiring data before and after a meal challenge to quantify the hyperemic postprandial response.

- Choose your sequence parameters carefully to best match the clinical question and the vasculature of interest

- Check the quality of the dataset before quantitative evaluation (e.g., conservation of mass analysis).

- There is a plethora of parameters that can be derived from 4D flow MRI, including the basic parameters such as velocity, instantaneous flow, and flow volume, as well as advanced parameters such as pulse wave velocity and wall shear stress.

Abdominal Applications

Liver:

- Typical 4D flow MRI findings in patients with cirrhosis include

  – a blunted post-prandial flow increase in the portal vein in response to a meal challenge.

  – increased azygos vein flow after a meal challenge indicating increased portosystemic shunting.

  – flow reversal in the portal vein, superior mesenteric vein, and/or splenic vein.

  – direct visualization and measurement of collateral flow.

- 4D flow MRI can detect gastroesophageal varices at high risk for bleeding through direct or indirect detection of flow reversal in the left gastric (coronary) vein.

- 4D flow MRI can be used for procedure planning and treatment monitoring up, e.g., for TIPS or living liver donors.

Aorta:

- 4D flow MRI could be used for risk assessment for progression and rupture in aortic aneurysms and dissections.

Kidneys:

- 4D flow MRI can be used for grading renal artery stenosis without the need of contrast media.

Gastrointestinal Tract

- A meal challenge can help diagnose chronic mesenteric ischemia through detection of a blunted increase in postprandial blood flow in the stenotic vessel or venous return to the liver via the SMV.

Placenta and Uterus:

- 4D flow MRI has the potential for early detection of increased risk for pregnancy complications through detection of a decrease in uterine artery blood flow rate in uterine vessels.
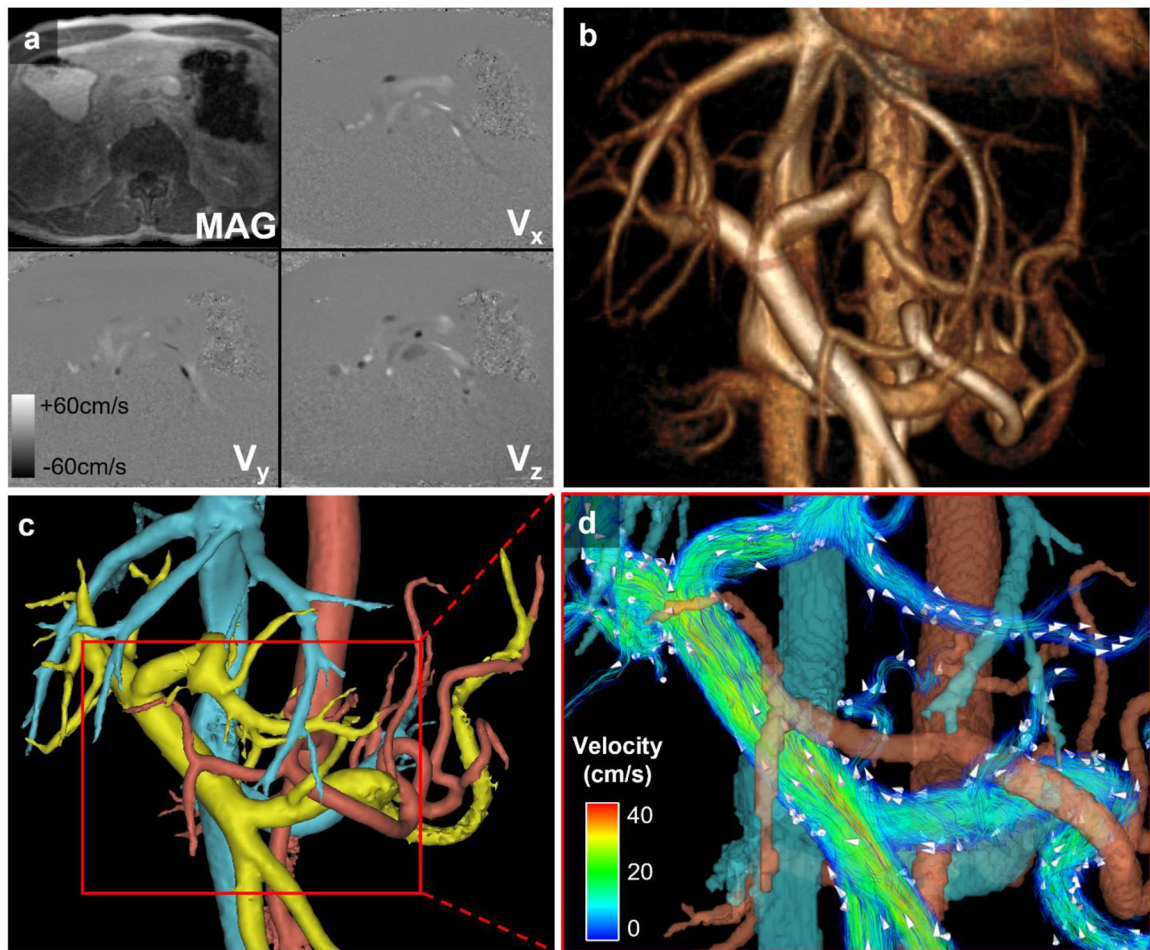
Fig. 1.
Post-processing workflow. (a) Source images: Time-averaged magnitude (MAG) and velocity images (Vx, Vy, Vz) from 4D flow MRI acquisition in a healthy volunteer shown for a single axial slice. (b) Volume-rendered angiogram of abdominal vasculature based on complex difference images. (c) Semi-automatically segmented colored masks of venous (blue), arterial (red), and portal (yellow) vasculature. (d) Quantitative and anatomical velocity information of the portal venous system portrayed via color-coded velocity streamlines. White arrows depict the direction of blood flow
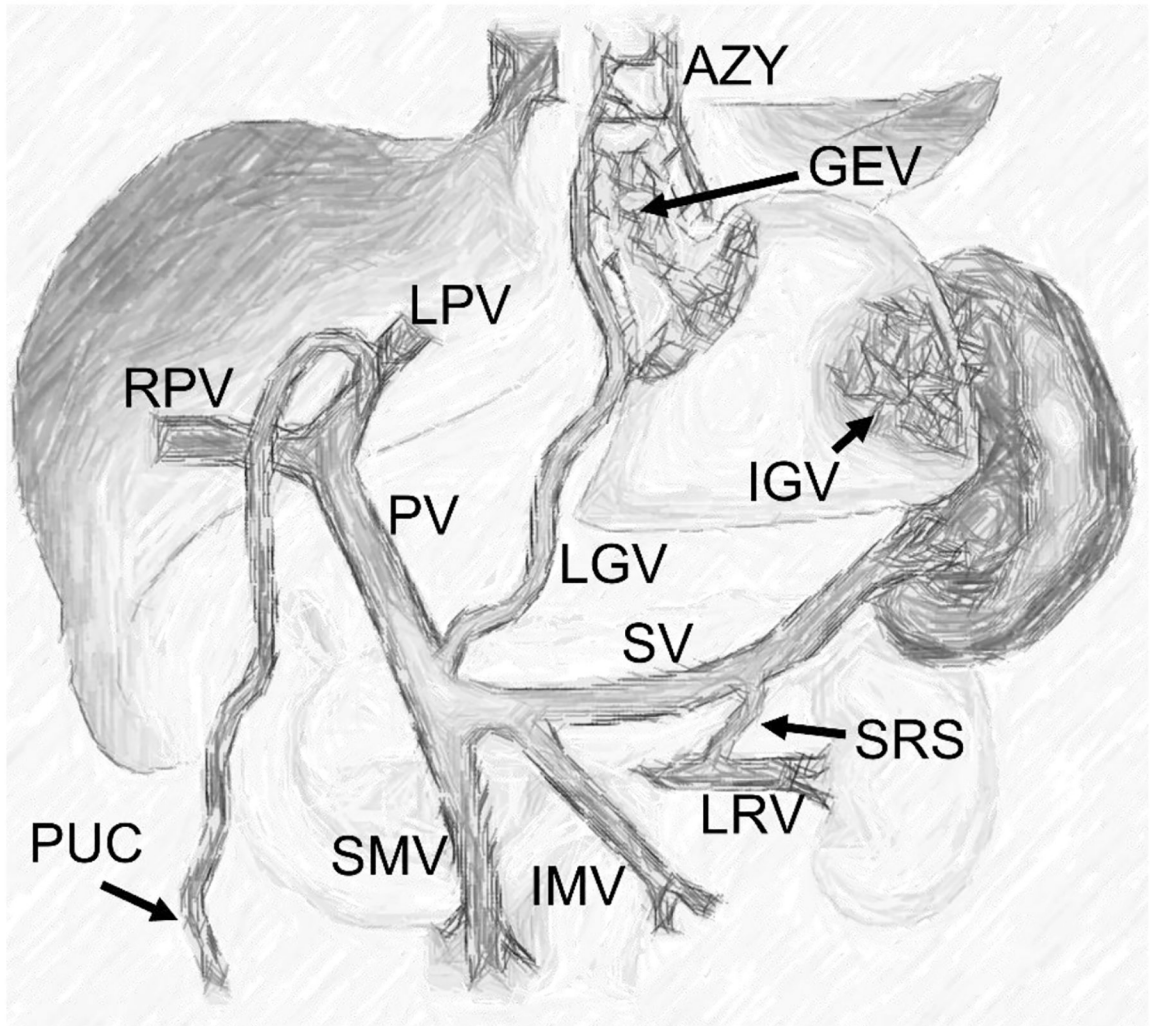
Fig. 2.
Anatomy of the portal venous circulation in portal hypertension. The schematic summarizes typical porto-systemic collaterals: Gastroesophageal varices (GEV) are fed by reversed flow in the left gastric vein (LGV) and drain into the azygos vein (AZY). Paraumbilical collaterals (PUC) are supplied by the left portal vein (LPV). Isolated gastric varices (IGV) are fed by the splenic circulation. A spontaneous splenorenal shunt (SRS) diverts flow from the splenic vein (SV) into the left renal vein (LRV). PV = portal vein, RPV = right portal vein, SMV = superior mesenteric vein, IMV = inferior mesenteric vein
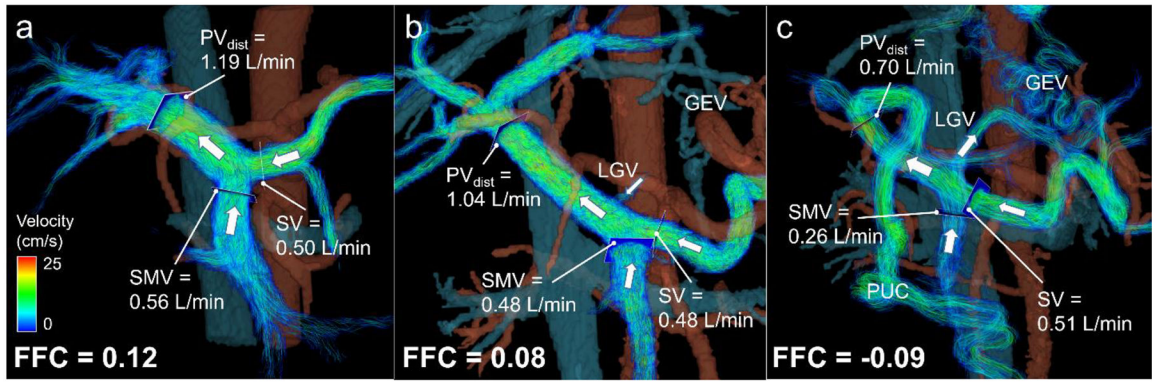
Fig. 3.
4D flow MRI for risk assessment of gastroesophageal varices in cirrhosis. To indirectly prove shunting to gastroesophageal varices (GEV), fractional flow change (FFC) can be computed as the difference in volumetric flow rates between the distal portal vein (PVdist) and the combined flow of the superior mesenteric vein (SMV) and splenic vein (SV) normalized to the sum of SMV and SV flow. Velocity color-coded streamlines visualize hemodynamics in the portal vasculature. Flow direction is indicated by white arrows. (a) Healthy 46-year-old female with normal anterograde flow in the superior mesenteric vein and splenic vein merging into the portal vein. (b) 64-year-old male with varices at a low risk of bleeding with severity assessed by endoscopy. In this case, the left gastric vein (LGV) could be visualized with normal hepatopetal flow into the portal vein. A positive FFC underlined the absence of hepatofugal flow indicating the absence of high-risk varices. (c) 54-year-old male with gastroesophageal varices at high-risk for bleeding. Hepatofugal flow was observed in the left gastric vein. Negative FFC reflected shunting to the gastroesophageal varices indicating varices at high-risk for bleeding. Note the presence of paraumbilical varices (PUC) draining blood from the left portal vein
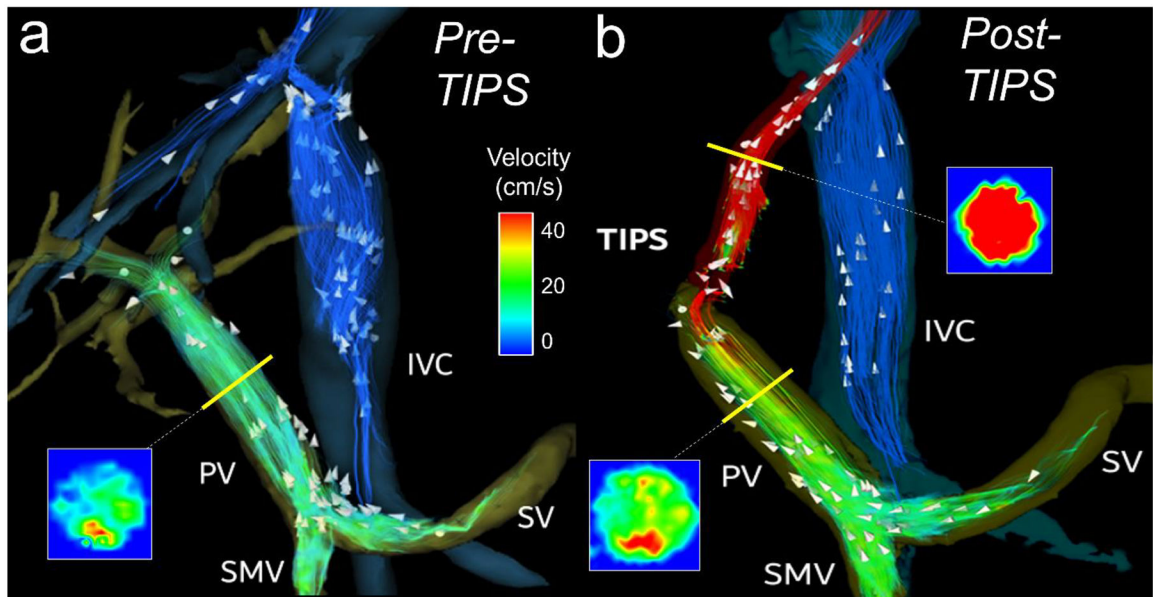
Fig. 4.
(a) 4D flow MRI velocity streamlines in portal vasculature prior to transjugular intrahepepatic portosystemic shunt (TIPS) placement in a 54-year-old male with nonalcoholic steatohepatitis. Blood flow volume in the portal vein was 0.94 L/min and peak velocity was 47 cm/s. (b) Streamlines two weeks after TIPS placement show subsequent increase in flow volume (2.4 L/min) and velocity (61 cm/s) in the portal vein as well as high flow (1.42 L/min) and peak velocity (108 cm/s) in the shunt. Note the signal dropout at the portal venous end of the stent graft due to disordered flow. TIPS therapy successfully reduced ascites. PV = portal vein, SMV = superior mesenteric vein, SV = splenic vein, IVC = Inferior vena cava
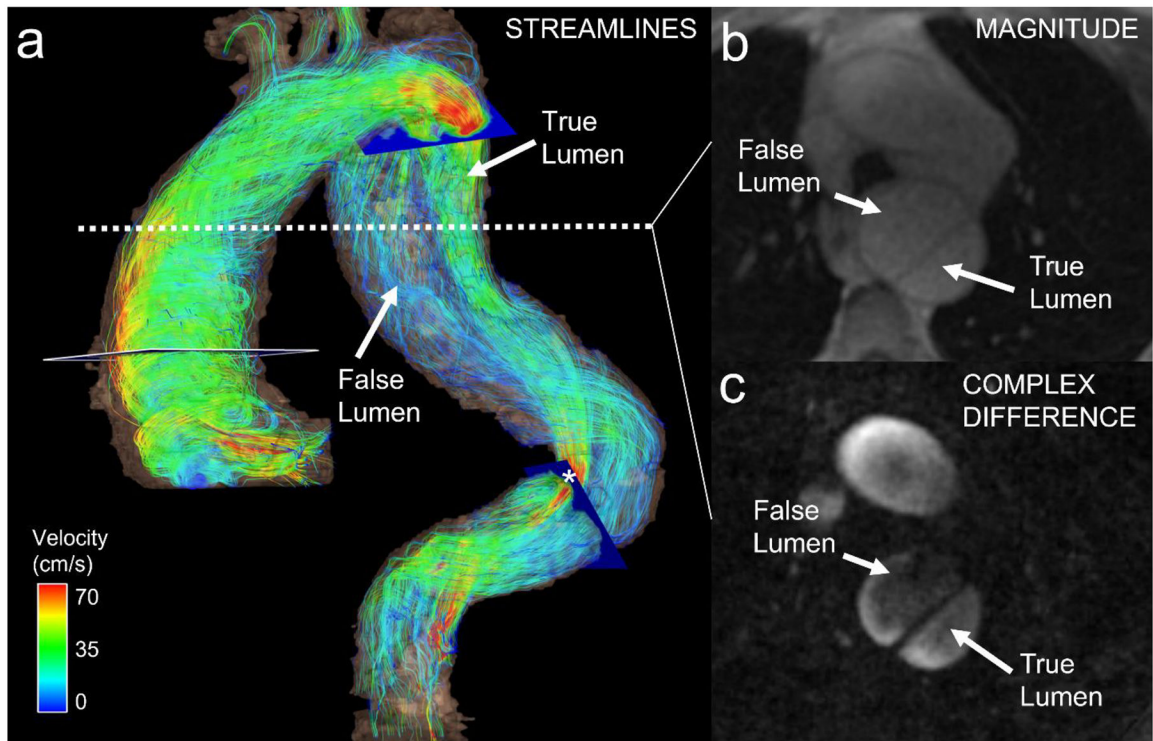
Fig. 5.
(a) Color-coded velocity streamlines (systolic phase) in a 71-year-old male with type B aortic dissection. Hemodynamics in both the true and false lumens could be visualized. Note lower velocities in the false lumen and focal flow acceleration in an area with relative stenosis of the true lumen (*). (b) Axial magnitude image and (c) complex difference angiogram from 4D flow MRI show dissection in descending aorta.
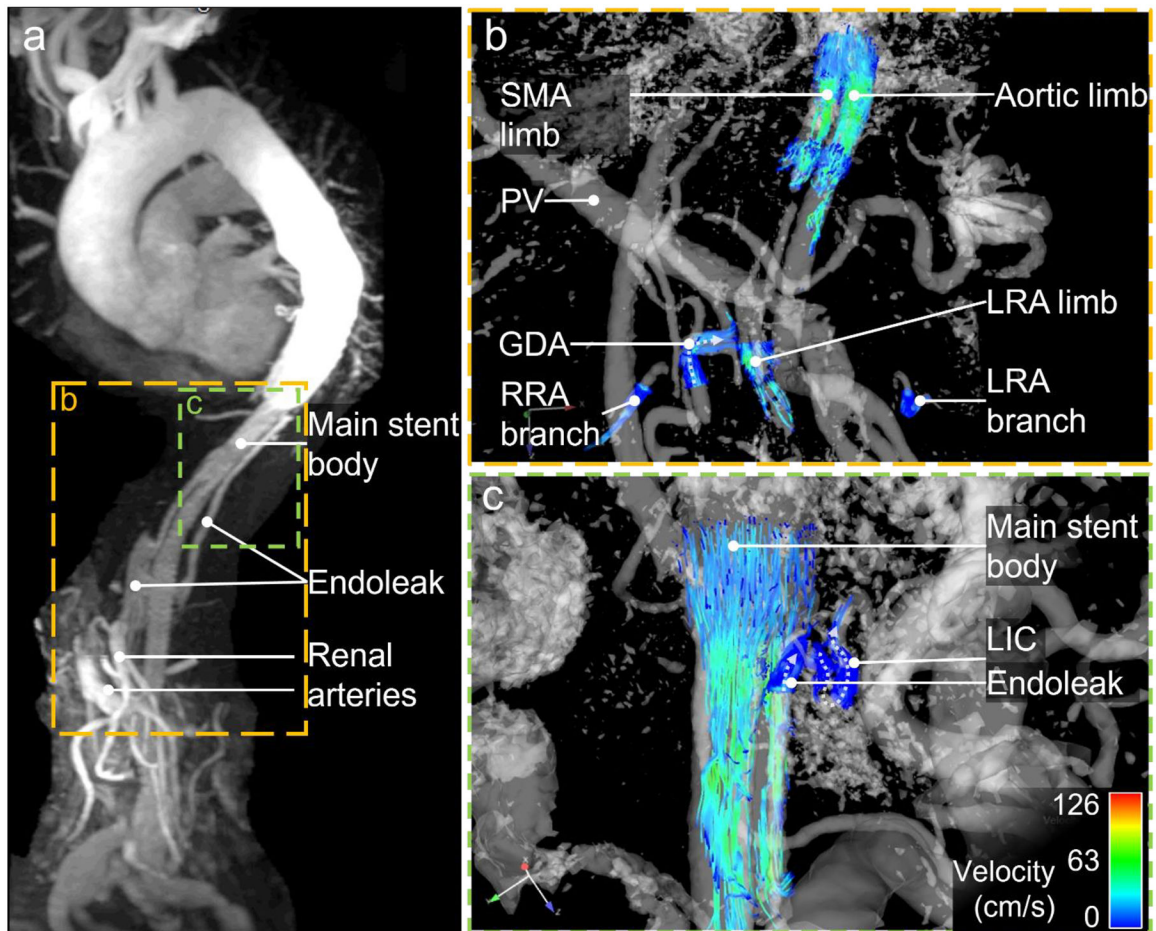
Fig. 6.
82-year-old after endovascular thoracoabdominal aneurysm repair with stent grafts in superior mesenteric artery (SMA), right and left renal artery (RRA, LRA, respectively). The celiac trunk was occluded with an intravascular plug. (a) Maximum intensity projection (MIP) of contrast enhanced MRA in parasagittal orientation depicts vessel morphology with endoleak. (b) 4D flow MRI in coronal orientation shows regular flow in branches of both renal arteries proving patency of both renal limbs. Retrograde flow within the gastroduodenal artery (GDA) supplies the celiac artery branches (flow direction marked with dotted arrow). (c) Streamlines show slow flow in caudo-cranial direction in the partially thrombosed aneurysm sack as well as antegrade flow in the left intercostal artery (LICA) draining the aneurysm sack. This proves that this intercostal artery is not feeding the aneurysm sack. Case courtesy of Dr. Christopher Francois, Mayo Clinic Rochester, Minnesota, USA
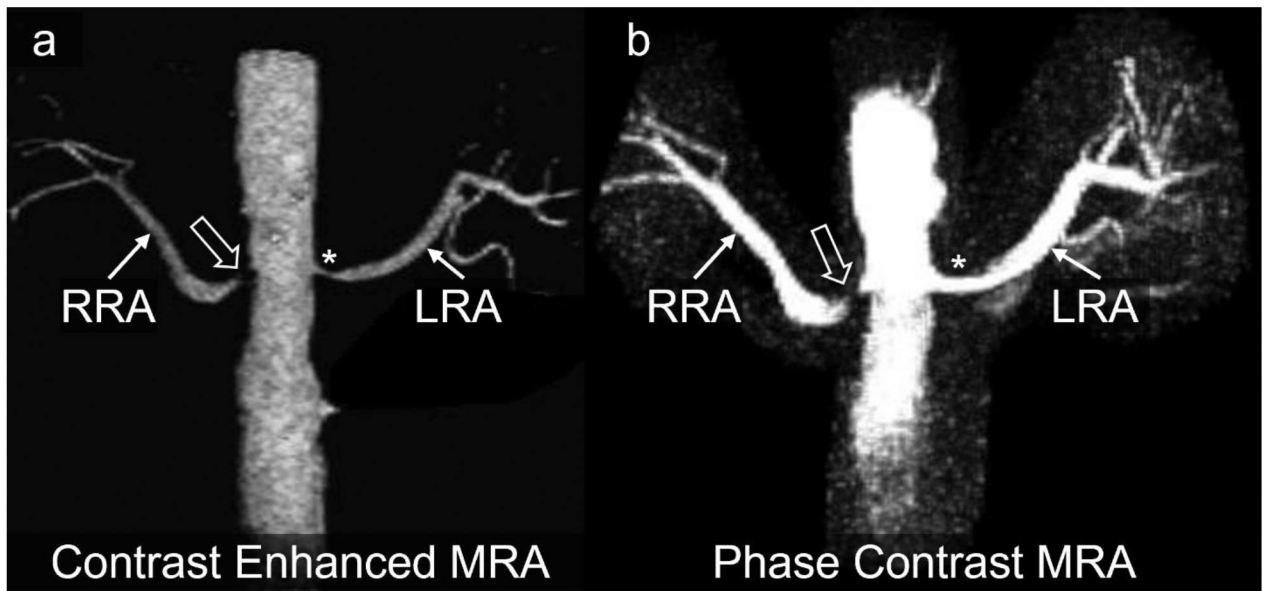
Fig. 7.
(a) Maximum intensity projection (MIP) of contrast enhanced MRA depicting severe stenosis (bold arrow) of the right renal artery (RRA) and moderate stenosis (Asterisk) of the left renal artery (LRA). (b) MIP of phase contrast MRA shows a signal dropout in the right renal artery stenosis indicating that this stenosis was hemodynamically significant. The stenosis of the left renal artery was not hemodynamically significant. Case courtesy of Dr. Christopher Francois, Mayo Clinic Rochester, Minnesota, USA
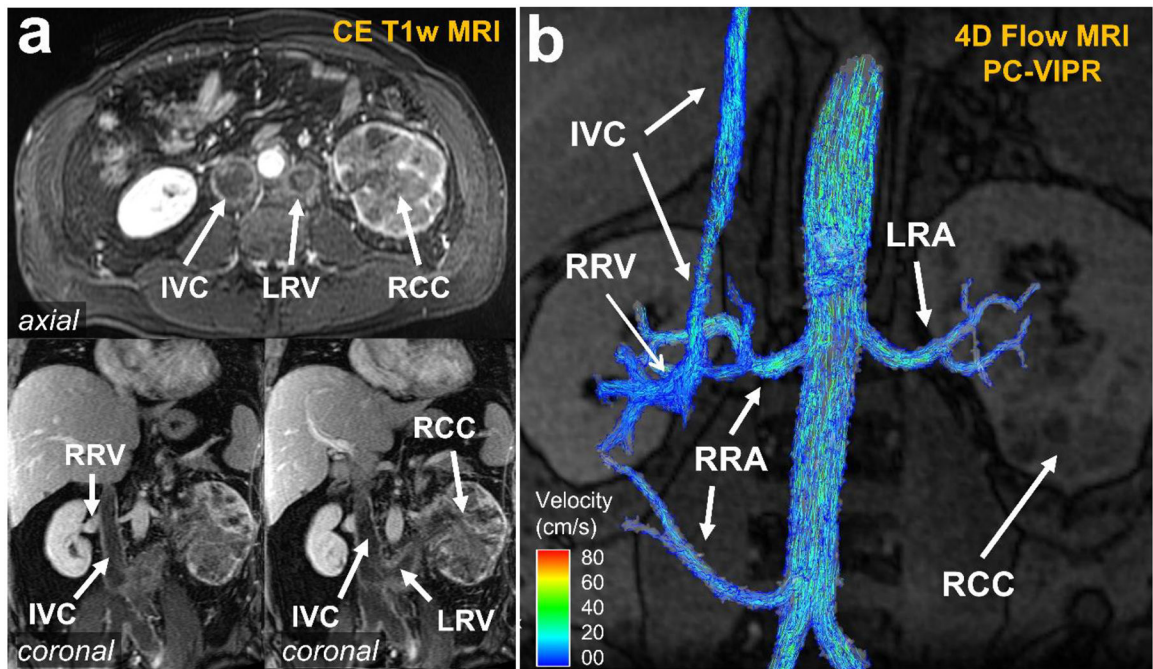
Fig. 8.
(a) Contrast-enhanced T1 MRI demonstrating renal cell carcinoma (RCC) of the left kidney with intravascular growth into the left renal vein (LRV) and the inferior vena cava (IVC). It is difficult to determine if the IVC has become fully occluded using only the T1-weighted images. Note the patent right renal vein (RRV) as comparison. (b) 4D flow MRI of right and left renal arteries (RRA, LRA, respectively): velocity streamlines confirmed that the IVC had a small patent section for venous return. This information is crucial for treatment planning
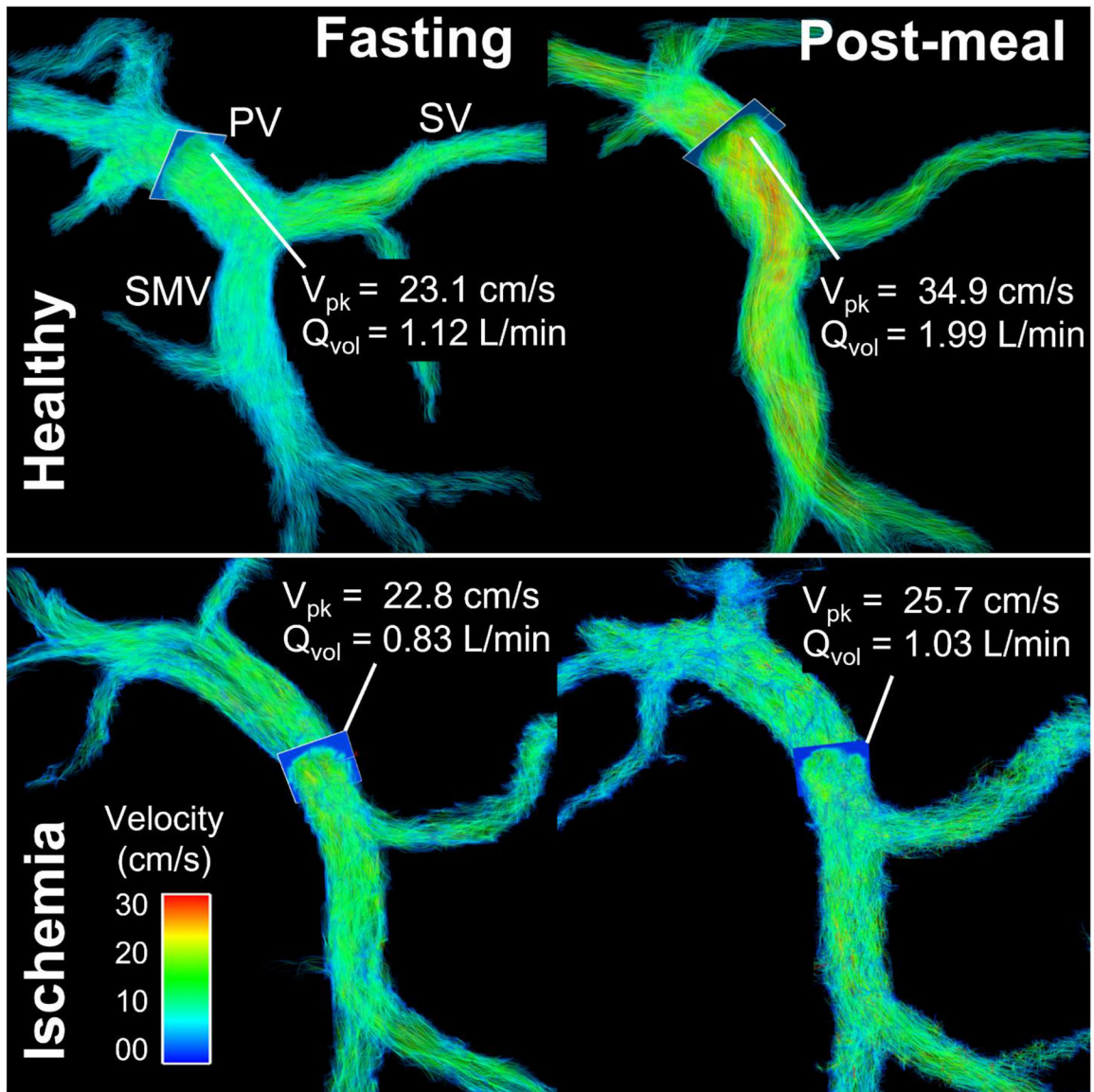
Fig. 9.
In a healthy volunteer (46-year-old female), flow volume (Q_{vol}) and peak velocity (V_{pk}) in the superior mesenteric vein (SMV) and portal vein (PV) increased markedly after a meal challenge draining blood from the gut. Simultaneously, flow in the splenic vein (SV) decreases slightly. In contrast, there was almost no flow or velocity increase in the portal venous system in a patient with chronic mesenteric ischemia (74-year-old female). The lack of physiological postprandial hyperemia of the intestines confirmed the diagnosis of chronic mesenteric ischemia
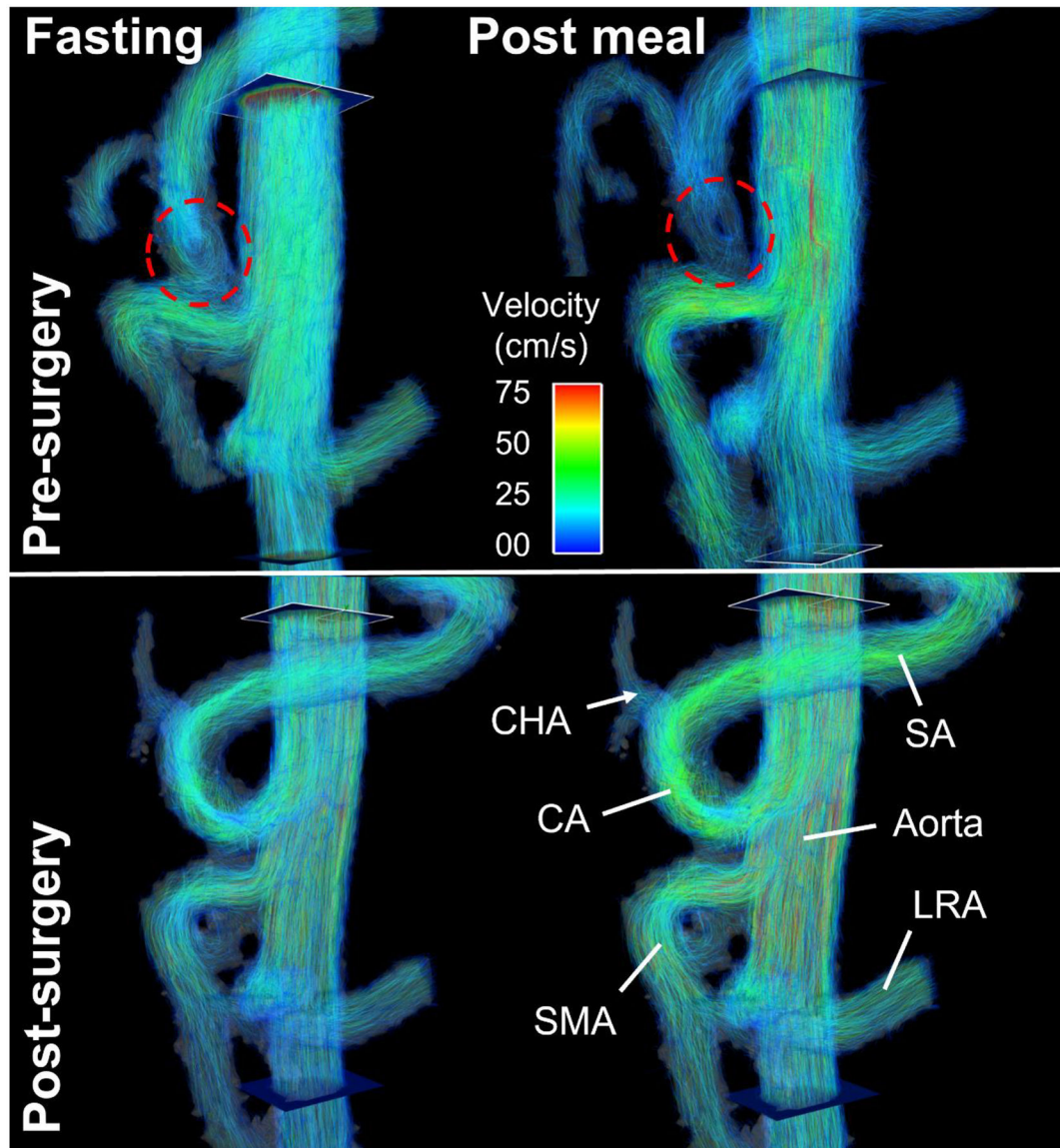
Fig. 10.

(Top) Compression of the celiac artery (CA, dashed red circle) caused by median arcuate ligament syndrome in a 22-year-old male before median arcuate ligament release. Velocity streamlines revealed slow vortical flow in the proximal celiac artery. Note the absence of postprandial flow increase in the celiac artery in contrast to the superior mesenteric artery (SMA). (Bottom) After decompression surgery, flow in the celiac artery increased markedly in fasting state with a distinct flow increase after a meal. CHA = common hepatic artery, SA = splenic artery, LRA = left renal artery
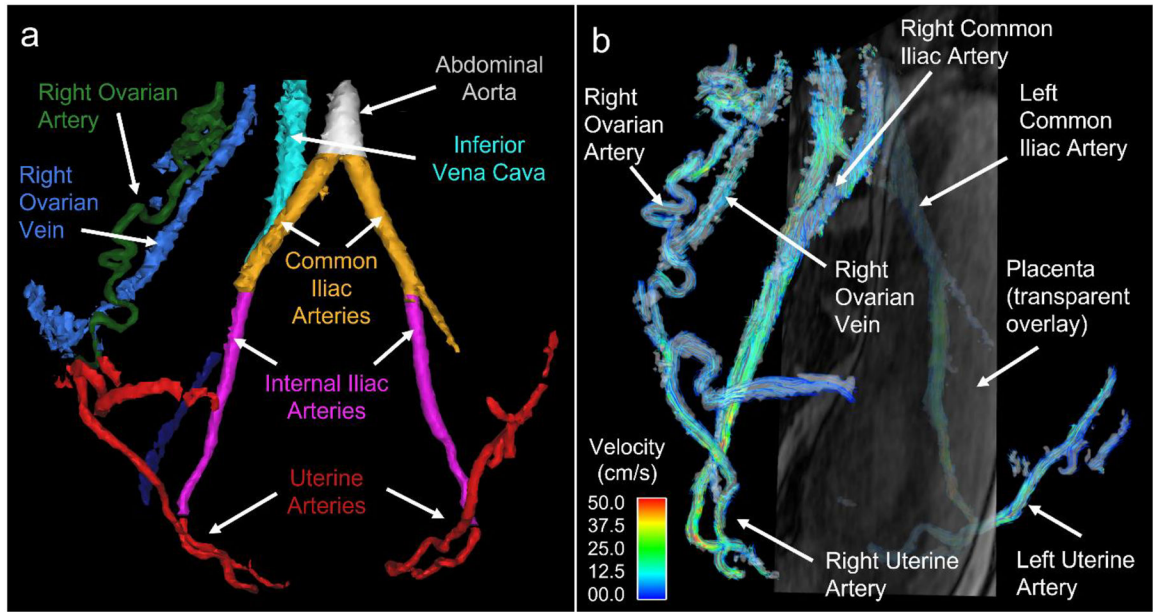
Fig. 11.
(a) Colored segmentation masks from a 4D flow complex difference angiogram show maternal vasculature at 20 weeks gestation. The uterine arteries (red) supply most of the blood to the placenta. The uterine branches of the ovarian arteries (right ovarian artery shown in green) can also contribute blood to the placenta. The left ovarian artery as well as much of the venous system is not shown. (b) Streamline visualization of flow in the maternal vasculature with a semi-transparent, sagittal magnitude image slice overlaid showing the uterus and placenta

Table 1

Typical characteristics of different angiography techniques of the abdomen. The given numbers are typical estimates for clinical routine cases based on the experience of the authors.

	4D flow MRI	2D flow MRI	MR angiography	CT	Ultrasound
Imaging characteristics					
Anatomical imaging	✓	✓	✓	✓	✓
Functional imaging	✓	✓	✓	-	✓
Time-resolved	✓	✓	✓	-	✓
Real-time imaging	-	-	-	-	✓
3D volume of interest	✓	-	✓	✓	-
Acquisition					
Temporal resolution	40 ms	20 ms	5000 ms	-	20 ms
In plane spatial resolution	1–3 mm2	1–2 mm2	1–3 mm2	~1mm2	1mm2
Contrast media required for routine imaging	-	-	✓	✓	-
Operator dependency	Low	High	Low	Low	High
Acquisition time	10–20 min free breathing	1 breath hold	1 breath hold	1 breath hold	20 min with breath holds
Analysis					
Postprocessing and analysis time	10–45 min	2–5min	0–5 min	0–5 min	-
Retrospective anatomical analysis of multiple vessels in volume of interest	✓	-	✓	✓	-
Retrospective functional analysis of multiple vessels in volume of interest	✓	-	-	-	-
Quantification of velocity	✓	✓	-	-	✓
Quantification of volumetric flow rate	✓	✓	-	-	-
Quantification of pressure differences	✓	✓	-	-	✓
Quantification of advanced parameters such as pulse wave velocity, shear stress	✓	-	-	-	-

Table 2

Typical acquisition parameters for human protocols

Vessel of interest	Spatial encoding	FOV (cm3)	In-plane spatial resolution / slice thickness (mm)	Temporal resolution in ms (number of time frames per cardiac cycle)	VENC (cm/s)	Acquisition time (min)
Portal venous system	Cartesian [6, 7, 9, 15, 19, 33]	22 × 32 × 8.6 [6]	1.3 – 3.2 / 1.3–4.0 (not specified if acquired or interpolated)	29 – 64 (9–20±1–7)	50–60 (TIPS: 80–225 [17, 37])	7–23±4–9
	Radial [12–14, 17, 34, 35]	32 × 32 × 22–32	1.25 – 1.4 isotropic (acquired)	43–71** (14)		10–12
Abdominal aorta	Cartesian [10, 26, 101, 106]	26–56 × 34–56 × 4.0–10.5	1.5–2.5 / 1.0–2.5 (acquired), or 2.4 / 2.5 (reconstructed)	35–83 (12–29)**	90–180 (or 10cm/s higher than peak velocity measured with 2D flow MRI)	5–15 [parallel imaging acc factor 2–5]
	Radial [8]	34 × 34 × 34	1.32 isotropic (acquired)	~72 (16)	150	11
Renal vessels	Cartesian [18]	40 × 40 × 12	2.5 / 5.0, reconstructed to 1.3 / 2.5	66–71 (8–15**)	Artery: 120 Vein: 45	2 × 3min acquisitions with different VENC settings
	Radial [112]	32 × 32 × 32	1.25 isotropic, reconstructed to 1.2 isotropic	30–50** (20)	20% higher than peak velocity measured with 2D flow MRI	9.5
Celiac trunk and superior mesenteric artery	Cartesian [19, 49]	20 × 24 × 3	1.5 –2.4 / 1.5–2.7 (acquired)	25–42** (24)	100–150 (healthy) 150–300 (with stenosis)	5–15 [k-t acc factor 5–8]
	Radial [14]	32 × 32 × 32	1.25 isotropic (acquired)	43–71** (14)	100 (preprandial), 120 (postprandial)	11
Uterine artery	Cartesian [119, 120]	32 × 20 × 6	1.25 isotropic (not specified if acquired or interpolated)	42–46 (10–18)	100 (50–200)	12–20 [PEAK-GRAPPA acc factor 4.7; no respiratory gating]
	Radial [121]	36 × 36 × 24	1.25 isotropic (acquired)	time averaged	60	10–12

Ranges or mean ± standard deviation are given depending on availability of data;

*
 FOV mentioned only in 1 study.

**
 if not given in the manuscript, temporal resolution was calculated for 60–100 bpm, based on given number of acquired time frames or vice versa. VENC, velocity encoding. Acc factor, accelerating factor.

Table 3

Potential clinical applications of abdominal 4D flow MRI

Organ	Clinical application	References
Liver	Cirrhosis: diagnosis and grading	Roldan-Alzate et al. 2016 [3], Stankovic et al. 2012 [6], Stankovic et al. 2010 [9], Roldan-Alzate et al. 2013 [12], Roldan-Alzate et al. 2015 [13], Motosugi et al. 2019 [34]
	Cirrhosis: identification of patients with increased risk for variceal bleeding	Motosugi et al. 2019 [34]
	Cirrhosis: identification of patients with severe hypersplenism	Keller et al. 2017 [19]
	Cirrhosis: evaluation of transjugular intrahepatic portosystemic shunts (TIPS)	Bannas et al. 2016 [17], Owen et al. 2018 [37], Stankovic et al. 2012 [95], Stankovic et al. 2015 [96]
	Surgical planning and follow up	Rutkowski et al. 2018 [98], Chiang et al. 2020 [100]
Aorta	Aortic dissections: prediction of progression and rupture risk	Liu et al. 2018 [101], Burris et al. 2020 [102]
	Characterization of hemodynamics in abdominal aortic aneurysms	Takehara et al. 2020 [10], Ziegler et al. 2019 [26], Sughimoto et al. 2016 [103]
	Identifying endoleaks and stenoses after endovascular aortic repair and predicting aneurysm sac expansion	Hope et al. 2009 [104], Takei et al. 2019 [105], Sakata et al. 2016 [106], Katahashi et al. 2019 [107], Salehi Ravesh et al. 2019 [108]
	Assessment of cardiovascular risk	Wentland et al. 2015 [63]
Kidneys	Detection and grading of renal artery stenosis	Francois et al. 2011 [16], Bley et al. 2011 [72], Ishikawa et al. 2015 [111]
	Assessment of kidney transplants	Bane et al. 2021 [18], Motoyama et al. 2017 [112]
	Surgical planning and surveillance of medical treatment	Takayama et al. 2014 [113]
Gastrointestinal tract	Diagnosis of chronic mesenteric ischemia	Roberts et al. 2021 [14], Hall Barrientos et al. 2021 [22], Siedek et al. 2018 [49]
Placenta and Uterus	Prediction of pregnancy complications	McKelvey et al. 2017 [116], Macdonald et al. 2019 [118], Hwuang et al. 2019 [119], Hwuang et al. 2020 [120]